GEOPHYSICS, VOL. 79, NO. 4 (JULY-AUGUST 2014); P. B151–B171, 22 FIGS., 2 TABLES.
10.1190/GEO2013-0171.1

Case History

An audio-magnetotelluric investigation of the Otjiwarongo and Katima Mulilo regions, Namibia

Pieter-Ewald Share[1], Alan G. Jones[2], Mark R. Muller[2], David T. Khoza[3], Marion P. Miensopust[4], and Susan J. Webb[5]

ABSTRACT

As an additional opportunistic component to the southern African magnetotelluric experiment, natural-source audio-magnetotelluric (AMT) data were acquired during phase IV to investigate the local-scale electric conductivity subsurface structure in the Otjiwarongo and Katima Mulilo regions (Namibia) as an aid in locating the installation points for high-voltage direct current earth electrodes. The study showed that the shallow subsurface of areas containing one measurement site in the Otjiwarongo region and three sites in the Katima Mulilo region have appropriate high conductivities for the optimal placement of the earth electrodes. Both of the AMT surveys are situated close to the edge of the orogenic Neo-Proterozoic Damara mobile belt (DMB). Previous studies all suggest the existence of a highly conductive midcrustal zone, which correlates well with the spatial location of the DMB. Two-dimensional inverse modeling of the Otjiwarongo AMT data confirms the existence of the high-conductive zone at midcrustal depths (10–15 km). The high conductivity of the DMB is explained by the presence of interconnected graphite in the marble units present. The Katima Mulilo inversion results are characterized by a conductive upper crustal layer that does not form part of the DMB conductive belt. It was deduced that at the uppermost subsurface (maximum ~200 m), Kalahari sediments are responsible for the high conductivity observed, whereas at greater depth (up to 6 km), its cause remains enigmatic, albeit the hypothesis of ironstone or graphite being present and causing the observed conductive upper crust.

INTRODUCTION

The southern African magnetotelluric experiment (SAMTEX) was a multinational project initiated in 2003 to study the electric conductivity subsurface structure of southern Africa by means of the magnetotelluric method (MT, Cagnaird, 1953; Chave and Jones, 2012), and to infer from it the tectonic processes involved in the formation of the southern African subcontinent (Figure 1). MT data were recorded at more than 740 locations covering an area that exceeds 1,000,000 km^2 (Jones et al., 2009b). The consortium members that formed SAMTEX come from academia, government, and industry (see the Acknowledgments in Jones et al., 2009b).

SAMTEX data have been used by various researchers in their scientific endeavors. There has been a comparison of electric and seismic anisotropy at lithospheric depths by means of analysis of MT data from SAMTEX and S-wave splitting of teleseismic

Manuscript received by the Editor 30 April 2013; revised manuscript received 15 January 2014; published online 27 May 2014.
[1]Formerly Dublin Institute for Advanced Studies, School of Cosmic Physics, Dublin, Ireland and University of the Witwatersrand Johannesburg, School of Geosciences, Johannesburg, South Africa; presently Council for Scientific and Industrial Research, Centre for Mining Innovation, Auckland Park. E-mail: pshare@csir.co.za.
[2]Dublin Institute for Advanced Studies, School of Cosmic Physics, Dublin, Ireland. E-mail: alan@cp.dias.ie; mark.muller@dias.ie.
[3]Formerly Dublin Institute for Advanced Studies, School of Cosmic Physics, Dublin, Ireland; presently Anglo American Technical Solutions and University of the Witwatersrand Johannesburg, School of Geosciences, Johannesburg, South Africa. E-mail: david.khoza@angloamerican.com.
[4]Formerly Dublin Institute for Advanced Studies, School of Cosmic Physics, Dublin, Ireland; presently Federal Institute for Geosciences and Natural Resources, Geozentrum Hannover, Hannover, Germany. E-mail: marion.miensopust@bgr.de.
[5]University of the Witwatersrand Johannesburg, School of Geosciences, Johannesburg, South Africa. E-mail: susan.webb@wits.ac.za.

events from a southern African seismic experiment (Hamilton et al., 2006), leading to a new model explaining the anisotropy observed at lithospheric depths in the Kaapvaal region. More recently, lithospheric 2D conductivity models have been produced for parts of South Africa, Namibia, and Botswana that indicate variations in conductivity between the older cratonic regions and younger surrounding mobile belts (Muller et al., 2009; Evans et al., 2011; Miensopust et al., 2011; Khoza et al., 2013). Furthermore, the conductivity models were used to make inferences about the thermal, mechanical, and chemical properties of the geologic terranes (Fullea et al., 2011) and to provide control on laboratory measurements of water in olivine (Jones et al., 2012). The correlation between diamond prospectivity and regional resistive/conductive boundaries in Namibia and South Africa has also been examined with SAMTEX results (Jones et al., 2009b; 2013; Muller et al., 2009).

During phase IV of SAMTEX, in conjunction with deeper probing of the earth, a study with shallower imaging objectives was undertaken in northern and northeastern Namibia. Two localized surveys were undertaken after a new consortium member, ABB of Sweden for NamPower of Namibia, expressed specific interest in the shallow subsurface in the regions close to the towns of Otjiwarongo and Katima Mulilo. The conductivity information in the Otjiwarongo and Katima Mulilo regions is needed for optimal placement of high-voltage direct current (HVDC) earth electrodes.

Owing to the shallow target depths under investigation, the high-frequency (typically 10–10,000 Hz) counterpart of MT and the audio-magnetotelluric (AMT) method were used. An AMT survey requires a dense spacing of sites to best define the extent of structures within the shallow subsurface (approximately 5 km). In the current study, the intersite spacing ranged from 5 to 20 km (Figures 2 and 3), in contrast to the minimum 20 km spacing for SAMTEX MT sites. AMT data were recorded at a total of 22 locations, of which 13 were situated in the Otjiwarongo region (Figure 2) and nine in the Katima Mulilo region (Figure 3). To provide greater depth resolution, broadband-magnetotelluric (BBMT) data (0.001–100 Hz) were also acquired at six of the 13 locations in

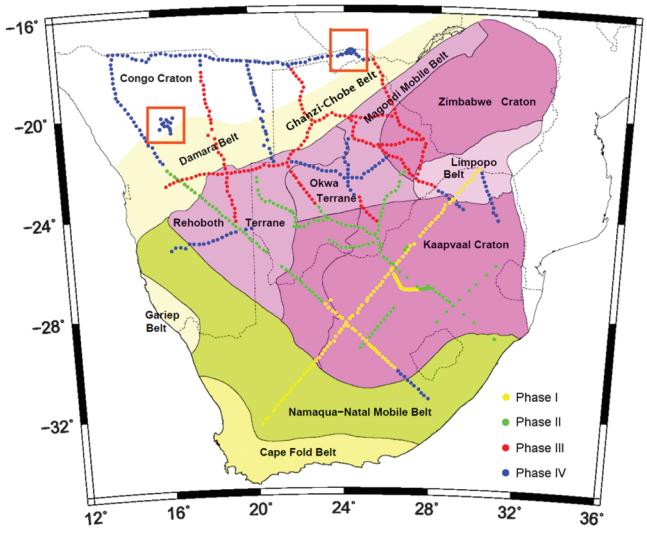

Figure 1. The more than 740 MT sites installed during SAMTEX plotted on a map of southern Africa's geologic provinces (after Nguuri et al., 2001). The two squares indicate the audio-magnetotelluric arrays installed close to the towns of Otjiwarongo (left) and Katima Mulilo (right) that are central to the current study.

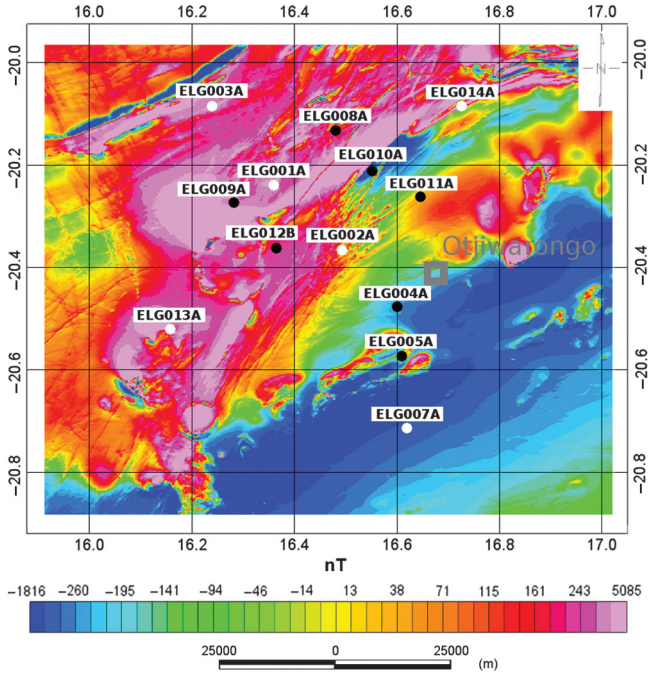

Figure 2. Locations of the 13 AMT sites installed during SAMTEX phase IV close to the town of Otjiwarongo, plotted on top of a high-resolution aeromagnetic map (200-m line spacing) of the area (courtesy of the Ministry of Mines and Energy, Geological Survey of Namibia). Sites ELG001A, ELG002A, ELG003A, ELG007A, ELG013A, and ELG014A have collocated BBMT and AMT data.

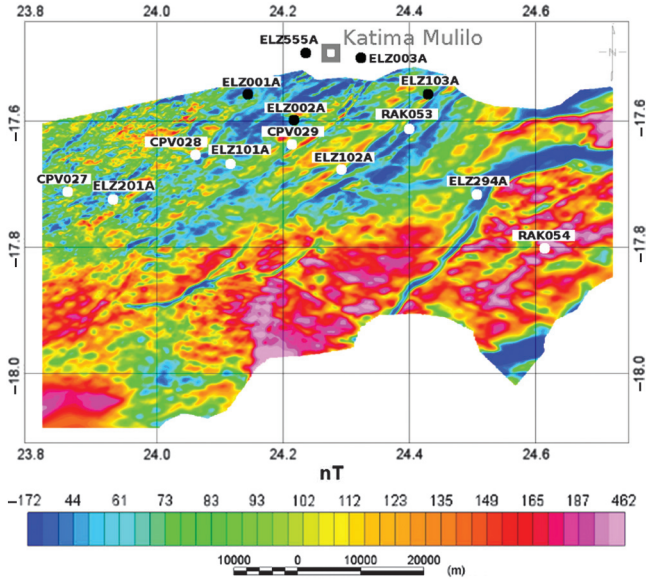

Figure 3. Locations of the nine AMT sites (site names starting with ELZ) installed during SAMTEX phase IV close to the town of Katima Mulilo, plotted on top of a high-resolution aeromagnetic map (200-m line spacing) of the area (courtesy of the Ministry of Mines and Energy, Geological Survey of Namibia). Sites ELZ101A, ELZ102A, ELZ201A, and ELZ204A have collocated BBMT and AMT data. The other sites shown, CPV027, CPV028, CPV029, RAK053, and RAK054, are BBMT sites also used in the current study and were installed prior to, or during, the installation of the AMT array.

the Otjiwarongo region, and four of the nine locations in the Katima Mulilo region.

The aim of the current study is to exploit the data from the two AMT arrays with existing modeling tools to find the best possible model of the subsurface conductivity structure for each area, up to midcrustal depths (20 km). Where available, BBMT data were used to resolve subsurface conductivity structure to even greater crustal depths. Modeling of MT data involves processing of the recorded electric and magnetic time-varying fields and obtaining appropriate frequency response curves for each site. The calculated responses are then analyzed for dimensionality and a choice of a 1D, 2D, or 3D inversion approach is made. In the present study, a 2D inversion approach is justified and deemed appropriate. Subsequently, galvanic distortion of the electric field is removed from the MT responses and geoelectric strike angles are obtained that best represent the regions' predominant 2D structural trends. The corrected responses are derived in the obtained strike angles and used as input to a 2D inversion algorithm (incorporated in the program WinGLink®) to obtain the subsurface conductivity models. After robust models (where all structures within the obtained models are required by the data) with low misfit errors are obtained, the results, together with models derived from other geophysical data sets, are correlated with existing geologic data to facilitate in constraining interpretation, where the geology is unknown. The conductivity models will also be used in recommending locations for the placement of the HVDC earth electrodes in the Otjiwarongo and Katima Mulilo regions.

GEOLOGY OF THE OTJIWARONGO AND KATIMA MULILO REGIONS

In general, the crust beneath the two study regions, and, in fact, for most parts of Namibia and Botswana (Singletary et al., 2003), consists of Neo-Proterozoic orogenic belts; the Damara belt in the Otjiwarongo region, and the Ghanzi-Chobe belt in the Katima Mulilo region. Large parts of the Damara belt are exposed in Namibia, but the Ghanzi-Chobe belt, except for a few sparse outcrops, is totally covered by Phanerozoic sediments. Geophysical data have in the past (Hutchins and Reeves, 1980) and present (SAMTEX) been used to investigate structures to crustal depths in the poorly exposed areas, and inferences about the geology underneath the sedimentary cover have been made. Through geophysical investigations, and the analysis of available geologic information, the Ghanzi-Chobe and Damara belts have been defined as interconnected (Key and Rundle, 1981) and is currently collectively termed the Damara mobile belt (DMB, Figure 1).

The DMB separates the composite Kalahari (Jacobs et al., 2008) and Congo (Begg et al., 2009) cratons in northern Namibia and Botswana, and was deposited during extensive rifting between the two cratons. Studies suggest initial deposition of Ghanzi-Chobe sediments (Modie, 2000), followed by later deposition of Damara sediments 1000–900 Ma (Tankard et al., 1982, p. 316) to at least 600 Ma (Miller, 1983). Apart from deposition, extensional faulting also took place during rifting between the Kalahari and Congo cratons and the faults were partly reactivated as thrusts during later continental collision (Miller, 1983). Today, the collisional thrusts manifest themselves as lineaments on the surface, and in southern Africa many observed regional lineaments are shear zones with large displacement (Coward and Daly, 1984). In the Damara belt specifically, shear zones separate regions of different stratigraphic and structural evolutions, in which its variability is primarily related to the different stages of deformation and metamorphism that took place across the belt (Miller, 1983; Daly, 1986). The four main zones identified in the Damara belt are the northern zone, central zone, southern zone, and southern margin zone (Gray et al., 2006). One of the major shear zones, separating the central and northern zones, is locally termed the Othohorongo thrust (Miller, 2008, p. 13–16, its southwest extension is called "Autseib Fault") and is located approximately 15 km south of the Otjiwarongo study region (Figure 4).

The Damara belt sequence consists of Archaean-Proterozoic basement outcrops, clastic sediments and minor volcanics of the Nosib group (1000–830 Ma) filling the fault-bounded troughs of rifted basement (Martin and Porada, 1977), carbonates of the Otavi group (830–760 Ma) rimming the ocean basins between cratons, turbidites of the Swakop group (830–760 Ma) within the ocean basins and foreland basin deposits of the Mulden and Nama groups (approximately 650 Ma, Gray et al., 2006) (Figure 4). The clastic sediments and carbonates of the Nosib and Otavi groups can be correlated with sequences in the Ghanzi group in northern Botswana (Ghanzi-Chobe belt). The Ghanzi group, together with volcanics of the Kgwebe formation (1100 Ma), which it disconformably overlies (Modie, 2000), constitute the rifted zone in northern Botswana. The northeast-trending metasedimentary and metaigneous rocks west of the rifted zone in Botswana are considered as extensions of the main part of the Damara belt in Botswana (Singletary et al., 2003). Due to the 300-m-thick sedimentary cover in northern Namibia and Botswana (Thomas and Shaw, 1990), it is difficult to state the exact basement composition beneath the Katima Mulilo study region. An extrapolation of geology from maps created using sparse outcrops, borehole data, and geophysical results in northern Botswana (Figure 5) into the Caprivi strip (a narrow eastward protrusion of Namibia separating Angola and Zambia from Botswana) shows the Kwando complex (Mesoproterozoic granite gneiss intrusion) and/or rocks of the Ghanzi group forming the basement beneath the Katima Mulilo study region. It is suggested (Catuneanu et al., 2005) that overlying these basement rocks in the study region are Karoo basin shales, sandstones, and weathered basalts, which are, in turn, overlain by the thick Kalahari sedimentary cover.

CRUSTAL ELECTRIC CONDUCTIVITY

Factors controlling conductivity

The extrinsic petrological and physical factors, on which conductivity is greatly dependant, are more easily explained and distinguished when coupled with the three conduction mechanisms (charge transport processes) present in the earth. The first conduction mechanism, electronic conduction, is important when highly conductive minerals (e.g., graphite, iron, or any metallic ore) form an interconnected or partially interconnected network within the host rock matrix (Nover, 2005). Another factor that influences conductivity is the presence of partial melt (Nover, 2005), which facilitates ionic conduction and generally explains high conductivities associated with volcanic areas. Its contribution to the total conductivity is directly related to the amount (melt fraction is dependent on temperature, Roberts and Tyburczy, 1999) and interconnectivity of the melts. The third conduction type, electrolytic conduction, dominates in fluid-filled porous rocks and varies with the petrophysical factors within the rock, namely, the size, orientation, interconnectivity, etc., of the pores and on the chemistry of the fluid and its interaction with the host rock (Nover, 2005). As with electronic

conduction and the presence of partial melt, the conductivity of fluid-filled porous rocks also depend on the amount and interconnectivity of the conducting phase (Jones, 1999). When no conductive phase is present, the final charge transport process, namely semiconduction, dominates. Semiconduction is most prominent in the earth's upper mantle and depends on thermodynamical factors such as temperature, oxygen fugacity (partial pressure of oxygen), and pressure to a lesser extent (Shankland, 1975; Jones et al., 2009a; Fullea et al., 2011).

Previous crustal conductivity studies in northern Namibia and Botswana

The first major investigation of the conductivity of northern Namibia and Botswana was a magnetovariational study in 1972 (de Beer et al., 1976). The study comprised 25 3C magnetometers spanning across an area that included central and northern Namibia, Botswana, and western Zimbabwe. The study resulted in the discovery of a long east–west-trending conductor crossing the survey area at depth. Characteristically, the magnetovariational method has poor depth resolution, and the surface outline of the conductor could only be accurately determined within an error that depends on the station spacing (50–150 km). Therefore, a second more dense magnetometer array covering only Namibia with a station spacing of approximately 60 km was installed in 1977 (de Beer et al., 1982) (Figure 6a). The greater spatial accuracy showed the conductor in Namibia to be curved rather than linear (Figure 6b), following the trend of the central zone of the DMB. Its depth, or more accurately depth to the anomalous induced currents flowing within it, was determined to be less than 45 km (de Beer et al., 1982). Installation of the magnetometer array was accompanied by several DC soundings using a Schlumberger configuration. These soundings inferred the top of the conductor to vary from 3 to 10 km (de Beer et al., 1982). In addition, inversions of the Schlumberger sounding curves inferred that the resistivity of the conductor was less than 20 Ωm and that of the surrounding upper crust ranged from 5000 to more than 20,000 Ωm.

In a more recent study, densely spaced (4–12 km) MT stations were deployed across the western end of the conductor (Figure 7a) by Ritter et al. (2003). Similar to earlier studies, an anomalous highly conductive middle to lower crust (resistivity as low as 5 Ωm) and a resistive upper crust (5000–15,000 Ωm) were detected (Ritter et al., 2003) (Figure 7b). In addition, the high-station density led to the discovery of anisotropic conductivities within, and parallel to, the Waterberg Fault/Omaruru Lineament (Weckmann et al., 2003), which is one of the tectonostratigraphic zone boundaries of the DMB (Figure 7b).

Van Zijl and de Beer (1983) suggest that the most plausible explanation for the high conductivity is the presence of serpentinite, thought to be the only rock that could develop the necessary high conductivity at midcrustal temperatures. Early experiments suggested that serpentine was conducting as a consequence of bound water (Stesky and Brace, 1973), but Olhoeft (1981) demonstrates that those results were in error, and the most recent ones show serpentine not intrinsically to be conducting (Reynard et al., 2011). There is, though, a highly conductive mineral associated with the process, namely, magnetite, and, if distributed appropriately on well-connected grain boundaries, it can drastically increase the conductivity of a rock (Pakhomenko et al., 1973). The process of serpentinization requires a large amount of water and van Zijl and de Beer (1983) admit explaining the origin of it during DMB formation, either originating from the mantle or being introduced by subduction, remains the only problem with the serpentinite

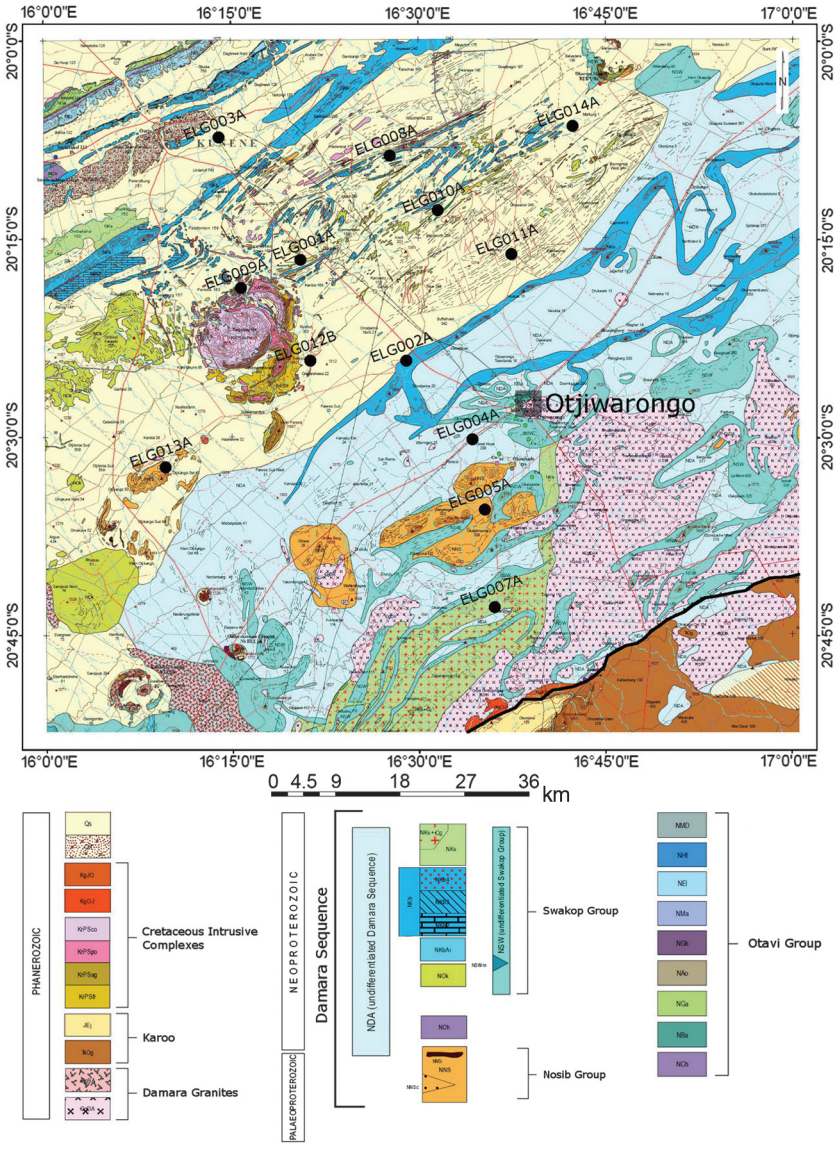

Figure 4. Locations of the 13 AMT sites installed in the Otjiwarongo region, plotted on top of a geologic map of the area (courtesy of the Ministry of Mines and Energy, Geological Survey of Namibia). The solid line in the southeastern corner of the map depicts the Othohorongo thrust.

model. Recent advances in understanding conductive anomalies at crustal depths point to the greater presence of fluids, fault gouge, sulfides, or graphite in shear zones as a more plausible explanation for the conductor (Ritter et al., 1999). Graphite-bearing marble units are widespread in the stratigraphy forming part of the conductor and Ritter et al. (2003) state that it is the most plausible cause of the high conductivity observed. Also, motion along shear planes is the ideal mechanism to ensure an interconnected network of conductive graphite over large distances.

DATA ANALYSIS AND INVERSION

AMT and collocated BBMT data

Programs included in the Phoenix Geophysics® software package were used for most of the data processing in the current study. The program SSMT2000 was used to precondition the time-series data, convert it from the time domain to frequency domain and calculate impedance estimates. Impedances were estimated using the stacking cascade decimation scheme incorporated into SSMT2000, which is identical to method four in Jones et al. (1989). In most cases, recording took place at a local site with at least one remote reference site recording simultaneously (see Gamble et al., 1979, for the remote referencing method). In all cases, where data from a remote site were available the remote magnetic fields were used in the impedance estimation of the local site, and where more than one remote site recorded simultaneously, multiple impedance estimates were obtained using data from each remote site. For logistical reasons, two AMT sites in the Otjiwarongo region, ELG002A and ELG004B, had no remote sites and were subsequently processed locally using their respective local magnetic fields.

The program MTeditor (also part of the Phoenix Geophysics package) was used to evaluate the calculated impedances and response curves. During evaluation, the remote-reference impedance estimate that was smoothest and contains the least amount of noise (if more than one estimate was available) was selected and outliers from the set of impedance estimates (calculated from the set of time sections) at each frequency were removed. At all sites, editing produced smoother, less noisy, and thus more reliable response curves. The one consistent poorly estimated frequency range that could also not be improved with editing was the AMT dead band (Garcia and Jones, 2002). After obtaining satisfactory response curves from all data at the location, the AMT responses with collocated BBMT data were merged (merged sites are hereinafter indicated by the letter m after the site name) and, together with the sites where either only AMT or only BBMT data were acquired, rotated from magnetic to true north.

Galvanic distortion removal and geoelectric strike analysis

Galvanic distortion is defined (Groom and Bahr, 1992; Utada and Munekane, 2000) as all the effects that charges accumulating on the surface of small (in an inductive sense) 3D heterogeneities, normally located close to the surface, have on the electromagnetic (EM) fields induced in larger background regional structures. In the present study, the removal of galvanic distortion and determination of geoelectric strike is done simultaneously, using an extended form of the classical Groom-Bailey decomposition (Groom and Bailey, 1989) developed by McNeice and Jones (2001), which is suited for multisite, multifrequency analysis. With the multisite, multifrequency analysis a global minimum misfit solution is sought to produce a geoelectric strike direction and galvanic distortion parameters for a range of frequencies and set of sites. Excluded in the determined galvanic distortion parameters is any frequency-independent scaling, otherwise known as static shifting, present in the impedance estimates. The code used in the current study for strike analysis that incorporates the extended form of the Groom-Bailey decomposition, is hereinafter referred to as *strike*.

First, to obtain an understanding of the dimensionality of subsurface conductivity structure in the Otjiwarongo and Katima Mulilo regions, the program strike was used to calculate a geoelectric strike angle for each site over all available frequencies (Figure 8a and 8b). In all calculations, an error floor of 3.5%, which corresponds to approximately 2° in phase and 7% in apparent resistivity, of the absolute value of the largest impedance was assigned to the calculated impedances. The program derives a strike angle that, together with the calculated distortion parameters, form part of a Groom-Bailey model (GB-model) that has the lowest possible misfit (GB-error) with the data. Given the assigned error floor, a GB-error of two or lower is defined as adequate for a calculated GB-model to

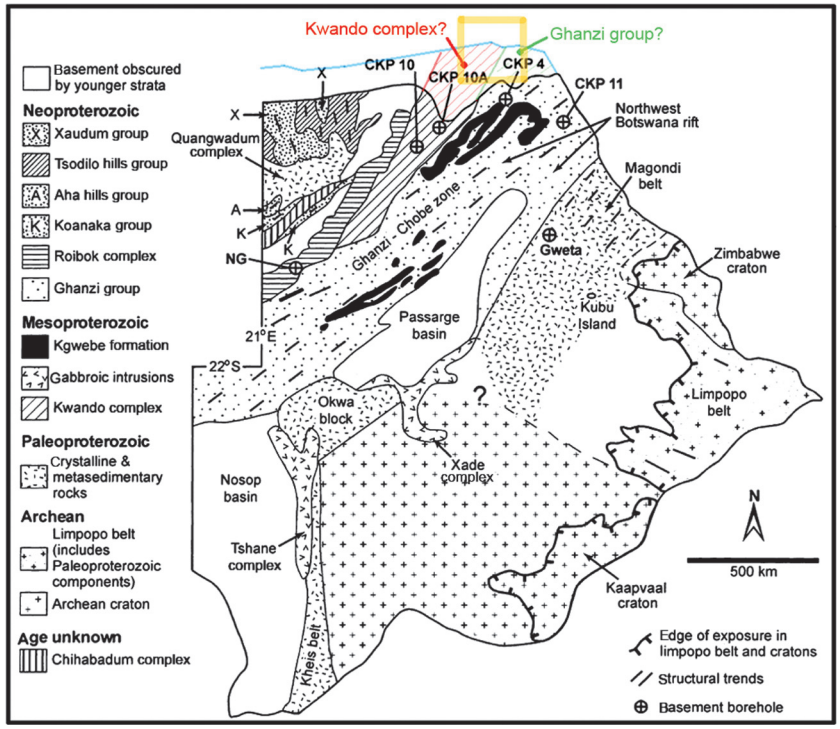

Figure 5. Subsurface Precambrian geology of Botswana, modified from Singletary et al. (2003), showing the probable extensions of Kwando complex and Ghanzi group rocks into the Caprivi strip (Namibia) and forming the basement beneath the Katima Mulilo study region (indicated by the square).

describe a measured data set; i.e., 95% of the model values lie within 2σ of the data estimates. A GB-error greater than two indicates (beside noisy data) that distortion is severe and/or the regional conductivity structure is 3D, and/or that the calculated errors are far too small. This is often a problem with parametric error estimates, especially when there are large numbers of estimates, because the assumption that each estimate is independent from all others and introduces new information is incorrect. Chave and Jones (1997) show that jackknife error estimates, which make no assumptions whatsoever about error distribution, are factors of 3–5 larger than parametric error estimates when there are large numbers of data.

Inherent to the MT method is a 90° ambiguity in the determination of strike that is resolved with external information such as geology and other geophysical data. In the Otjiwarongo region, the calculated strike angles were rotated, if needed, by 90° to align as best possible with structural trends in geology (Figure 4) and regional magnetic data (Figure 2). Due to thick sedimentary cover in the Katima Mulilo region, no structural information was available, and regional magnetic data were used to remove the ambiguity in strike determination (Figure 3).

Most of the GB-errors associated with the single site strike analysis in the Otjiwarongo region are at or below two; therefore, the assumption of a 2D regional structure for each individual site is valid (Figure 8a). In the Katima Mulilo region, all the GB-errors associated with the single site strike analysis are also at or below two (Figure 8b), thus, the 2D assumption is also valid. In addition, because many sites have small average phase differences between the transverse electric (TE, horizontal electric field is polarized, and currents flow, parallel to dominant strike) and transverse magnetic (TM, horizontal magnetic field is polarized parallel to dominant strike and current flows 90° to it) modes (Figure 8b), a 1D inversion can even provide a good approximation of the regional conductivity structure.

To further investigate the conductivity substructure of, first, the Otjiwarongo region, and in an effort to find a single strike angle that fits the Otjiwarongo data, the data were rotated to user-defined strike directions in increments of 10°, with the aim of observing changes in GB-errors with rotation. The interesting result was that for all rotations the GB-errors at each individual site remained approximately equal (Figure 9 shows the constant GB-errors for 0°, 20°, 40°, 60°, and 80°). GB-errors calculated for the rotation of site ELG005s data from 0° to 90° showed the largest variation, with a standard deviation of 0.43. At all the other sites, a standard deviation of 0.26 or lower was derived. It was concluded that the small change in errors indicate that each site contains, for most of the available frequencies, data with associated GB-errors that remain largely unchanged by rotation (approximately 1D). The problem of finding a strike angle for the Otjiwarongo region is now reduced

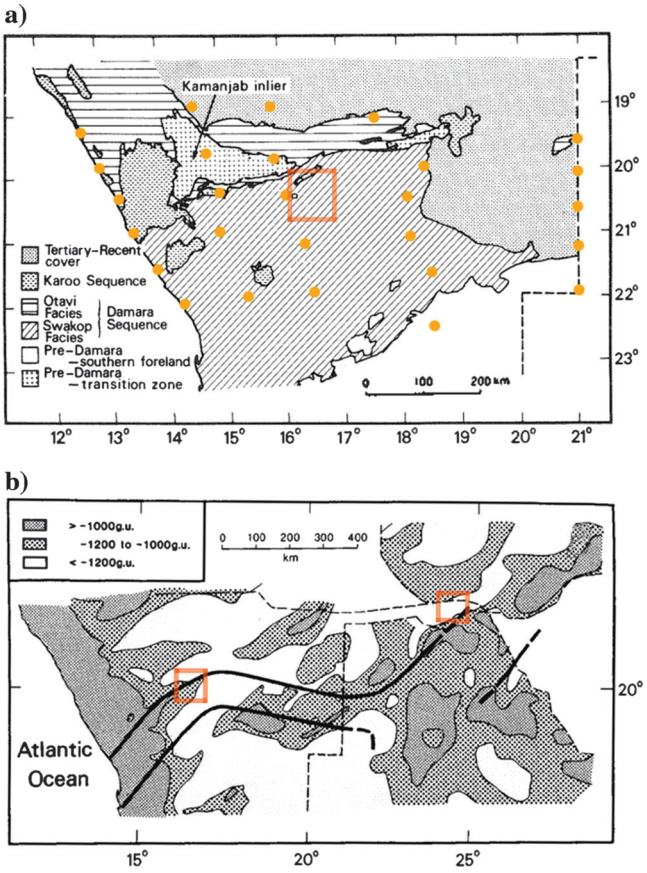

Figure 6. The dense 1977 magnetometer array (dots) relative to regional geology in Namibia [(a), Otjiwarongo study region indicated], and the proposed conductor, determined with the 1972 and 1977 arrays and Schlumberger sounding data (see text), crossing mainly Namibia and Botswana, in relation to a simplified Bouguer anomaly map [(b), the Otjiwarongo and Katima Mulilo study regions are indicated] (van Zijl and de Beer, 1983).

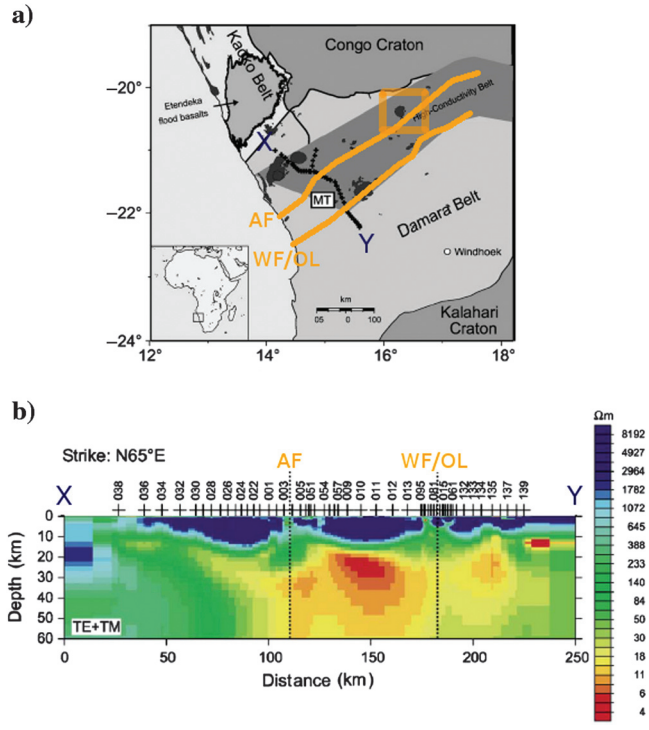

Figure 7. (a) The DMB sandwiched between the Kalahari and Congo cratons in Namibia and the 1998–1999 MT profile (*x*–*y*, Ritter et al., 2003) crossing the conductive belt. Post-Karoo alkaline igneous complexes are indicated in dark gray, and (b) 2D MT inversion results showing the highly conductive middle crust in the central part of the profile and the resistive upper crust. AF denotes the Autseib Fault and WF/OL denotes the Waterberg Fault/Omaruru Lineament (Ritter et al., 2003).

to identifying the frequencies at each site that have higher dimensional characteristics and calculating an average strike angle using only the identified higher dimensional data.

In the Otjiwarongo region, data from each site were analyzed decade-by-decade, by assigning strike angles from 0° to 90° to each decade independently and observing the associated change in GB-errors with the changes in angle. Only the decades characterized by GB-errors that remain greater than two for most angles and then drop below the tolerance level of two within some angle range were selected for further strike analysis. In total, 62 frequency decades from the 13 Otjiwarongo sites were analyzed and only nine decades from eight sites passed the criterion for higher dimensionality. Due to the consistently poor impedance estimates in the AMT dead band, the decade 10,000–1000 Hz was not considered for further analysis, even if it appeared to have 2D characteristics. The eight sites, their frequency decades that were determined to be higher dimensional, and the strike angles computed using strike are listed in Table 1 and depicted graphically in Figure 10a. Only one frequency decade (100–10 Hz, ELG002m in Table 1) has a GB-error greater than two. Thus, as before, it can be concluded that the data predominantly sense 1D and 2D subsurface structures and the continued analyses of data using 2D modeling tools is justified. After examining the eight groups of frequencies, it was determined that there exists no overlapping frequency or Niblett-Bostick depth (NB-depth, Niblett and Sayn-Wittgenstein, 1960; Bostick, 1977; Jones, 1983a) range among them. Subsequently, strike could not be used, in multisite mode, to compute a common strike angle for the eight sites. Consequently, a single strike angle was obtained by calculating a simple arithmetic average of the eight strike estimates. Averaging the eight strike angles computed produced a value of 82°, and the corresponding average GB-error for all 13 Otjiwarongo sites in the resultant strike direction was 1.86.

The single site strike analysis of the Katima Mulilo data demonstrated that there is a high degree of one-dimensionality in the region. Therefore, upon rotation of the data, the consistency in GB-errors, similar to the Otjiwarongo data, was expected. Subsequently, the same decade-for-decade analysis applied in the Otjiwarongo region was used to analyze the Katima Mulilo data to extract minor parts of higher dimensional data from the predominantly 1D data. In total, 65 frequency decades (from 14 Katima Mulilo sites) were analyzed and only 12 from seven sites passed the criterion for higher dimensionality. The seven sites, their frequency decades that were determined to be higher dimensional, and the strike angles computed using strike, are listed in Table 1 and depicted graphically in Figure 10b. At all but one of the sites a GB-error less than two is achieved (ELZ102m, Table 1). Again, no common frequency or NB-depth range could be established and an arithmetic average of the seven values was calculated to obtain a representative strike angle for the Katima Mulilo region. The resultant average was 54°, and the corresponding average GB-error for all 14 Katima Mulilo sites in the resultant strike direction was 1.12.

2D inversions of Otjiwarongo and Katima Mulilo data

In the current study, all 2D conductivity models were derived from inversions of the Otjiwarongo and Katima Mulilo data using the algorithm by Rodi and Mackie (2001), as implemented in the WinGLink software package. The algorithm minimizes a function that includes a data misfit and a regularization term, usually taken to be a smoothing term. In WinGLink, the main user-definable variable, which controls the amount of regularization (smoothing), is denoted by τ. In addition, the regularization can be alternated between minimization of the Laplacian and minimization of the gradient of the model. It is also possible to specify either a uniform grid or standard grid Laplacian regularization to be applied on the created meshes.

In the Otjiwarongo and Katima Mulilo regions, the acquisition of data in a semiarray format lead to 2D inversion profiles (orientated perpendicularly to obtained strike angles) being placed in regions where the site density was highest. The Otjiwarongo sites nearest to the chosen profile, and included in the inversion process, were ELG007m, ELG005, ELG004, ELG002m, ELG012, ELG009, ELG001m, and ELG008 (Figure 11a). The sites included in the Katima Mulilo 2D inversion were RAK054, ELZ294, RAK053, ELZ102m, CPV029, ELZ002, ELZ555, and ELZ001 (Figure 11b). In both cases, if two sites, after projection took place, located at the

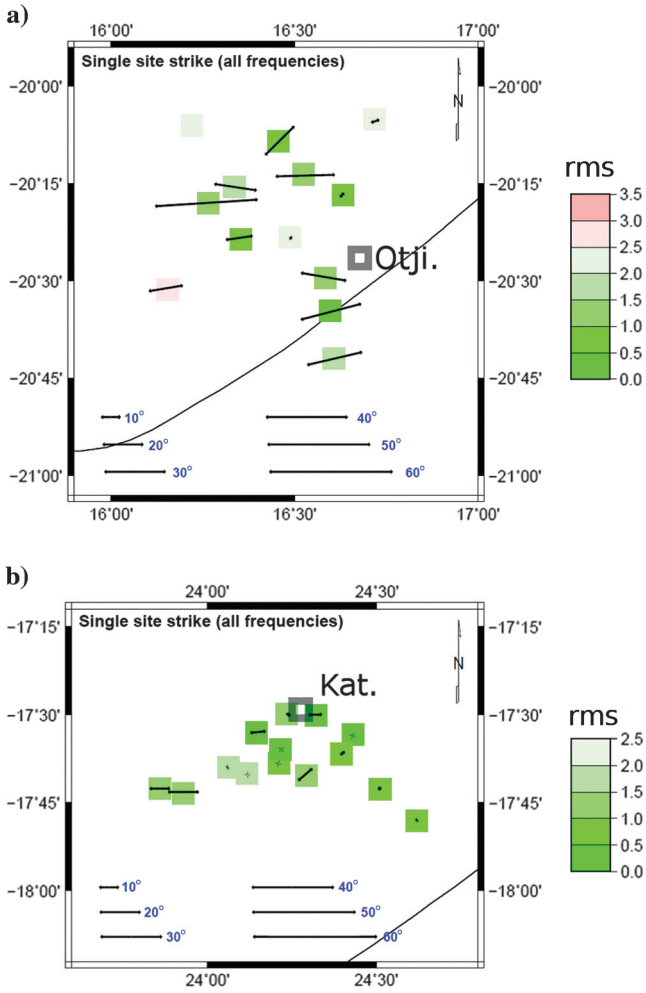

Figure 8. Strike angles computed for each individual MT site in the (a) Otjiwarongo (Otji. denotes Otjiwarongo) and (b) Katima Mulilo regions (Kat. denotes Katima Mulilo) over all the available frequencies. The colors of the boxes indicate the GB-errors (root mean square — rms) for each calculation of strike and the arrow lengths depict the phase differences between TE and TM modes at each site. The northeast-trending line is a prominent intra-DMB magnetic feature and represents the dominant structural trend in the area.

same point on the profile then the farthest one from the profile was excluded during inversion.

For the construction of meshes for the two inversions the following general guidelines were followed:

1) The first horizontal gridline was placed approximately half the smallest EM skin depth of all the sites from the surface. A horizontal line represented the surface, as no significant elevation changes were observed in either the Otjiwarongo or Katima Mulilo area.
2) In accordance with the loss in resolution with increasing depth as EM energy diffuses into the earth, each successive horizontal gridline was separated from the previous one by a distance that gradually increased with depth.
3) The array format of sites meant that intersite spacing was irregular after projection of sites onto a profile. Subsequently, the density of vertical gridlines was made highest around site locations (on the profile) and less dense in between, and away from, sites, in accordance with the fact that resolution decreases laterally away from an observation point with decreasing frequency.
4) All horizontal and vertical gridlines assigned to a 2D plane were done such that the aspect ratios (length-to-width ratio) of the rectangular cells remained reasonable. A reasonable aspect ratio, in this case, is one that is not less than 0.025 and not greater than 40.

For all inversions, uniform 100 Ωm half-spaces were used as starting models. Also, minimization of the Laplacian (default option) was selected because, although minimizing the gradient produces a smoother model, the same smoothness can be obtained by selecting the default option and varying the other regularization parameters. A regularization trade-off curve (Hansen, 1992), which is optimally L-shaped, was used to obtain the most appropriate smoothing operator τ for each set of inversions. Similar approaches have been used in seismology (Boschi et al., 2006) and MT (Schwalenberg et al., 2002). Trade-off curves were constructed for the Otjiwarongo and Katima Mulilo data by gradually decreasing τ from 100 to 1, running a smooth 2D inversion for each of the τ values, and plotting the resultant rms errors versus τ values. TE and TM modes were inverted for, and, by assigning much larger error floors to the apparent resistivities than the phases, emphasis on fit was placed predominantly on phase (phase values are not affected by static shifts). Uniform grid and standard grid Laplacian options, with the default α and β selected, were used to construct the trade-off curves. As an example, the curve for the uniform grid Laplacian inversions of the Otjiwarongo data is shown in Figure 12, and the point ($\tau = 20$) indicative of the optimal regularization value for these inversions is highlighted. Similarly, after analyses of the remaining curves, a τ value of seven was selected for all subsequent standard grid Laplacian inversions of the Otjiwarongo data, and a τ value of 10 was used for all inversions of the Katima Mulilo data.

The optimal α and β values to use in the standard grid Laplacian inversions of the two data sets were selected by noting how the rms errors of inversions varied as different pairs of weighting parameters were used, and selecting the pair that gave the smallest rms error (Table 2). TE and TM modes (with equal error floors) as well as apparent resistivities and phases were inverted for. During inversions to determine the appropriate α and β values, and all inversions mentioned henceforth, phase data are inverted for first, by, as before, assigning larger error floors to the apparent resistivity estimates than the phase data. Thus, the effect of static shifts on initial inversions is effectively zero. During succeeding inversion runs, the apparent resistivity error floors are lowered, and the initial models are modified by the additional constraint of requiring a minimal misfit to the apparent resistivity data as well. As the apparent resistivity error floors are lowered, the option to invert for static shifts is selected (zero summation of the natural logarithm of all computed static shift factors is required at each iteration, de Groot-Hedlin, 1991). Such a sequence of inversions, results in models that are least biased by static shifts. For both standard grid Laplacian inversions of the Otjiwarongo and Katima Mulilo data α and

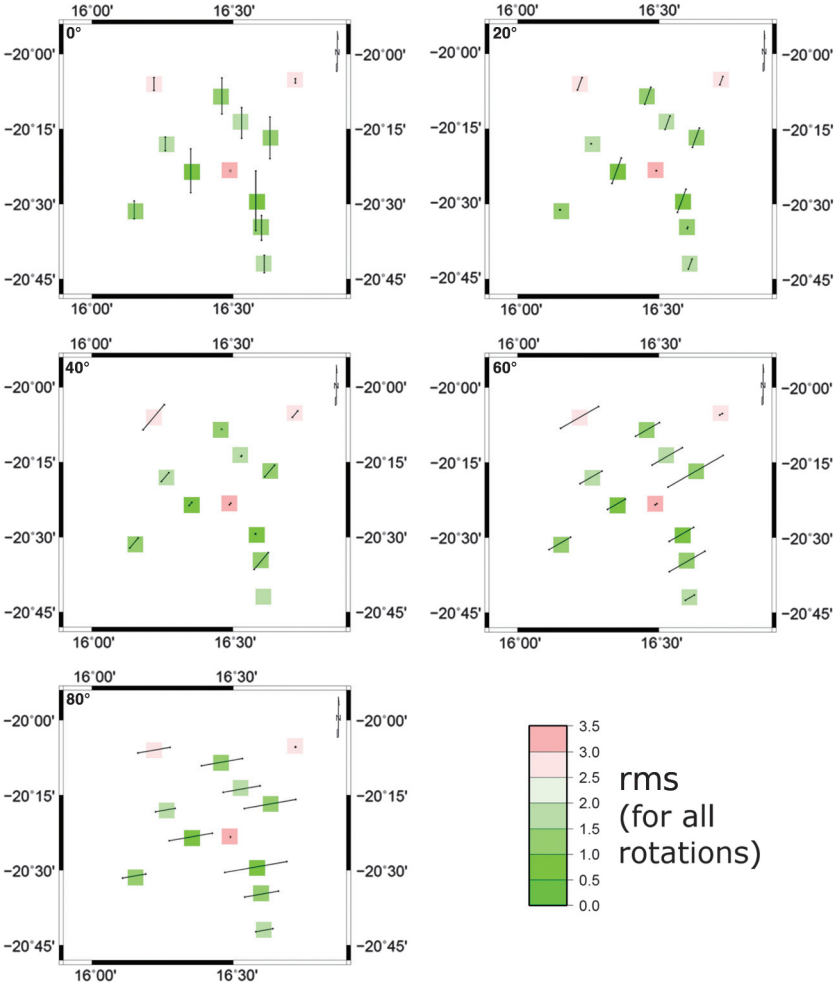

Figure 9. GB-errors (rms) and phase differences computed after assigning strike angles of 0°, 20°, 40°, 60°, and 80° to data from the Otjiwarongo region.

β values of one and three, respectively, produced the lowest rms errors and were subsequently used in all further standard grid Laplacian inversions (Table 2). Owing to the equal weighting assigned to all cells when using uniform grid Laplacian regularization, α and β values were kept at the default values of one and one, respectively, and H and V remained 0 and 0 m, respectively.

To observe the unique information given by the TE and TM modes in the Otjiwarongo and Katima Mulilo regions, respectively, the two modes were initially independently inverted (Figures 13 and 14). The variations in penetration depths for each mode were also calculated (Figures 13 and 14). In each case, the error floors assigned to the apparent resistivities and phases of the two modes were 8% and 3%, respectively, and static shifts were inverted for. Earlier studies indicated that the TM mode is generally more robust to the effects of surficial 3D bodies than the TE mode (Jones, 1983b; Wannamaker et al., 1984). More recent studies show that the greater robustness of the TM mode mostly applies to conductive 3D features (Berdichevsky, 1999). In addition, Berdichevsky (1999) also points out that for resistive 3D features both modes are equally robust, whereas in some geologic models, such as a 3D resistive horst, it is even possible that the TE mode is the more robust component.

The standard grid Laplacian inversions of the Otjiwarongo data gave much larger rms errors fitting the TE mode responses rather than the TM mode ones (Figure 13). It is, therefore, concluded that the TE mode is more affected by surface 3D features, and in particular conductive 3D features. In contrast, the uniform grid Laplacian inversion of the TM mode responses gives a larger rms error than the TE mode inversion (Figure 13). The smoothness constraints placed on the inversion using uniform grid Laplacian regularization counteracts the unique information provided by the TM mode, thus the higher TM rms error is ascribed to regularization. The equal TE and TM rms errors of the standard grid Laplacian inversions of the Katima Mulilo data (Figure 14) show that either the modes are unaffected by 3D features or both are affected by, and are equally robust to, resistive 3D features present. Again, selecting uniform grid Laplacian regularization resulted in the TM mode inversion of the Katima Mulilo data having a higher rms error than the TE mode inversion (Figure 14). It should also be noted that structures appearing below the penetration depth of each site (NB-depths in Figures 13 and 14) are not sensed by the data and are, in fact, regularization effects and were subsequently removed from further models (Figure 15 onwards).

During joint inversion of the TE and TM modes of the Otjiwarongo data, and using standard grid Laplacian regularization, error floors of 10% and 5% as well as 8% and 3% were selected for the TE apparent resistivities and phases and TM apparent resistivities

Table 1. The eight selected Otjiwarongo and seven selected Katima Mulilo sites (see text), their frequency decades determined to be higher dimensional, the strike angles computed for the identified decades and the GB-errors (rms) associated with each computation.

	Frequencies (Hz)	Strike (°)	GB-error
Otjiwarongo sites			
ELG001m	1–0.1	80.02	0.89
ELG002m	100–10	43.66	2.57
ELG003	10–1	53.14	1.64
ELG005	10–1	75.77	0.71
ELG007m	10–1	73.49	0.44
ELG009	10–1	94.77	0.88
ELG013m	100–10	109.42	0.54
ELG014m	10–0.1	93.32	1.44
Katima Mulilo sites			
CPV028	1–0.001	57.51	1.92
ELZ101m	1–0.1	54.87	1.50
ELZ102m	1–0.01	48.69	2.53
ELZ201m	1–0.1	92.57	1.10
ELZ294	0.1–0.01	57.81	0.34
RAK053	0.1–0.001	51.45	1.47
RAK054	1–0.01	54.72	0.35

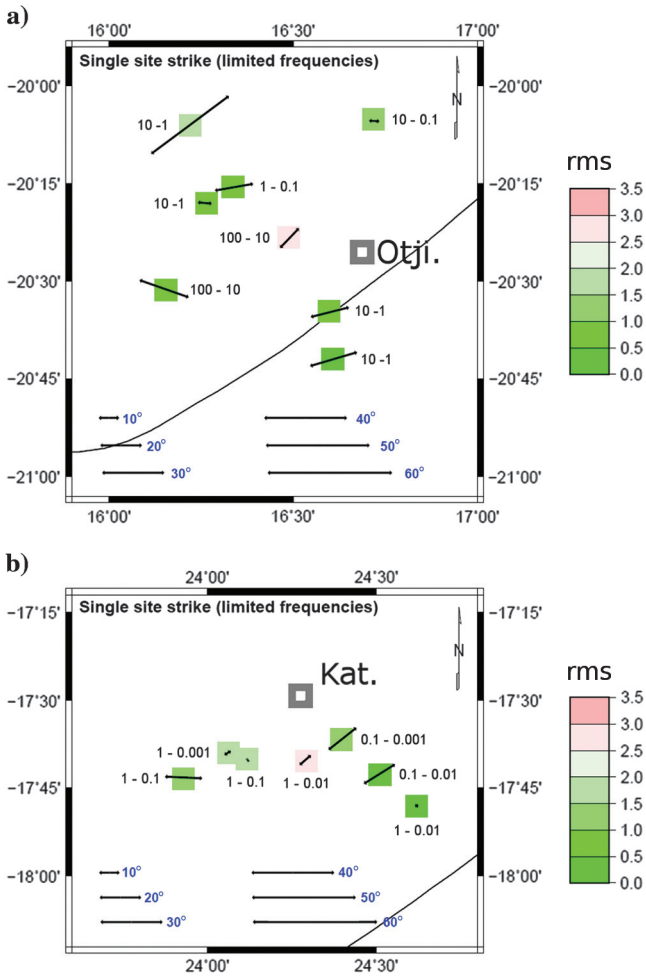

Figure 10. Strike angles (arrow directions in boxes), GB-errors (rms, box colors), and phase differences (arrow lengths in boxes) for the eight Otjiwarongo (a) and seven Katima Mulilo (b) sites, which passed the higher dimensional criterion, computed over the limited number of frequencies that have higher dimensional characteristics. The frequency ranges of each site are indicated as well (e.g., 1–0.1 means 1–0.1 Hz).

and phases, respectively (Figure 15). The selection of larger TE mode error floors ensures the preferential minimization of misfit between model and TM mode data, which are less sensitive to 3D surficial structures, during each iteration. To improve the rms error of the joint TE and TM mode inversion, when using uniform grid Laplacian regularization, error floors of 8% and 3% as well as 10% and 5% were assigned to the TE apparent resistivities and phases and TM apparent resistivities and phases, respectively (Figure 15). Using the same error floors, a uniform grid Laplacian inversion with τ set to seven was also completed with the purpose of comparing standard grid and uniform grid Laplacian joint inversions of the Otjiwarongo data where equal smoothing factors are used (Figure 15). The equal rms errors of the individual TE and TM mode standard grid Laplacian inversions (Figure 14) of the Katima Mulilo data resulted in the apparent resistivities and phases of both the modes being assigned equal error floors of 8% and 3%, respectively, during joint inversion (Figure 16). Error floors of 8% and 3% as well as 10% and 5% were assigned to the TE and TM apparent resistivities and phases, respectively, of the Katima Mulilo data during joint uniform grid Laplacian inversion (Figure 16). For all inversions, except for the standard grid Laplacian inversion of the Katima Mulilo data, the order in which the TE and TM components were added to the inversion that resulted in the lowest possible rms was TE phase, TM phase, TE apparent resistivity, and TM apparent resistivity; for the standard grid Katima Mulilo inversion the TM phases were added before TE phases. Therefore, phase first inversions, and the inversion for static shift when the apparent resistivity data are added, simultaneously give the lowest rms errors and guarantee models that are least biased by static shifting.

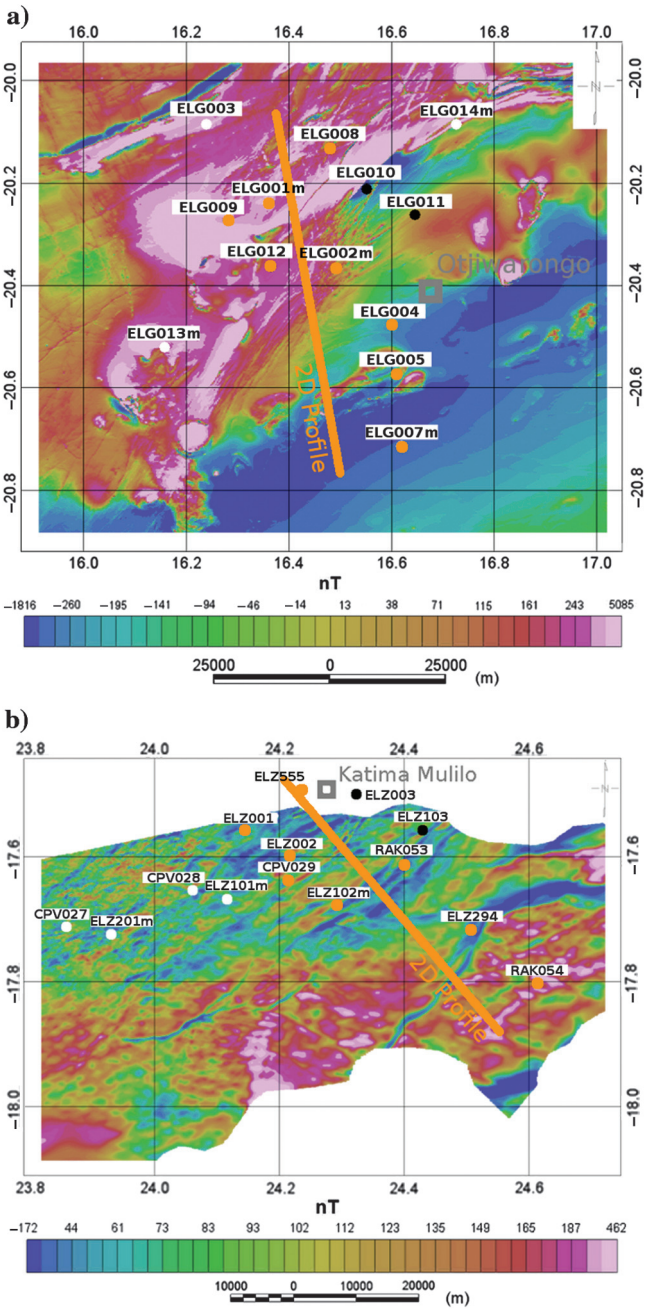

Figure 11. Two-dimensional inversion profiles created perpendicular to the 82° and 54° average strike directions in the Otjiwarongo (a) and Katima Mulilo (b) regions, respectively. The eight sites included in the 2D inversion of each region are indicated.

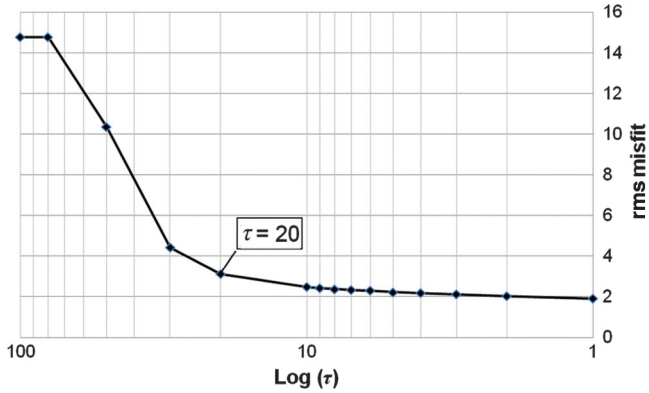

Figure 12. Regularization trade-off curve (plot of rms misfit versus log [τ]) for the uniform grid Laplacian inversions of the Otjiwarongo data. The optimal τ value of 20 is indicated.

Table 2. The rms errors for inversions of the Otjiwarongo and Katima Mulilo data using standard grid Laplacian regularization and varying weighting parameters α and β. The H and V were both kept at the default value of 500 m. The absence of entries for some Katima Mulilo inversions indicates that there was no convergence of the inversion algorithm for the α and β values shown.

	$\beta = 1$	$\beta = 2$	$\beta = 3$	
Otjiwarongo	4.10	3.39	2.96	$\alpha = 1$
	4.36	3.69	3.55	$\alpha = 2$
	4.81	3.84	3.57	$\alpha = 3$
Katima Mulilo	4.99	3.76	2.52	$\alpha = 1$
	4.74	–	–	$\alpha = 2$
	–	–	–	$\alpha = 3$

SENSITIVITY TESTING

A comparison of the two uniform grid Laplacian inversions with $\tau = 20$ (Figure 15b) and $\tau = 7$ (Figure 15c) shows that in general the same conductive and resistive structures are present, but that the resistivities of the structures differ between models. Owing to the stated similarities and to better compare uniform and standard grid Laplacian inversions of the Otjiwarongo data, where model differences are not due to different τ-values, the uniform grid Laplacian inversion with $\tau = 7$ is used in further analysis. A site-for-site misfit comparison between the two Otjiwarongo inversions in

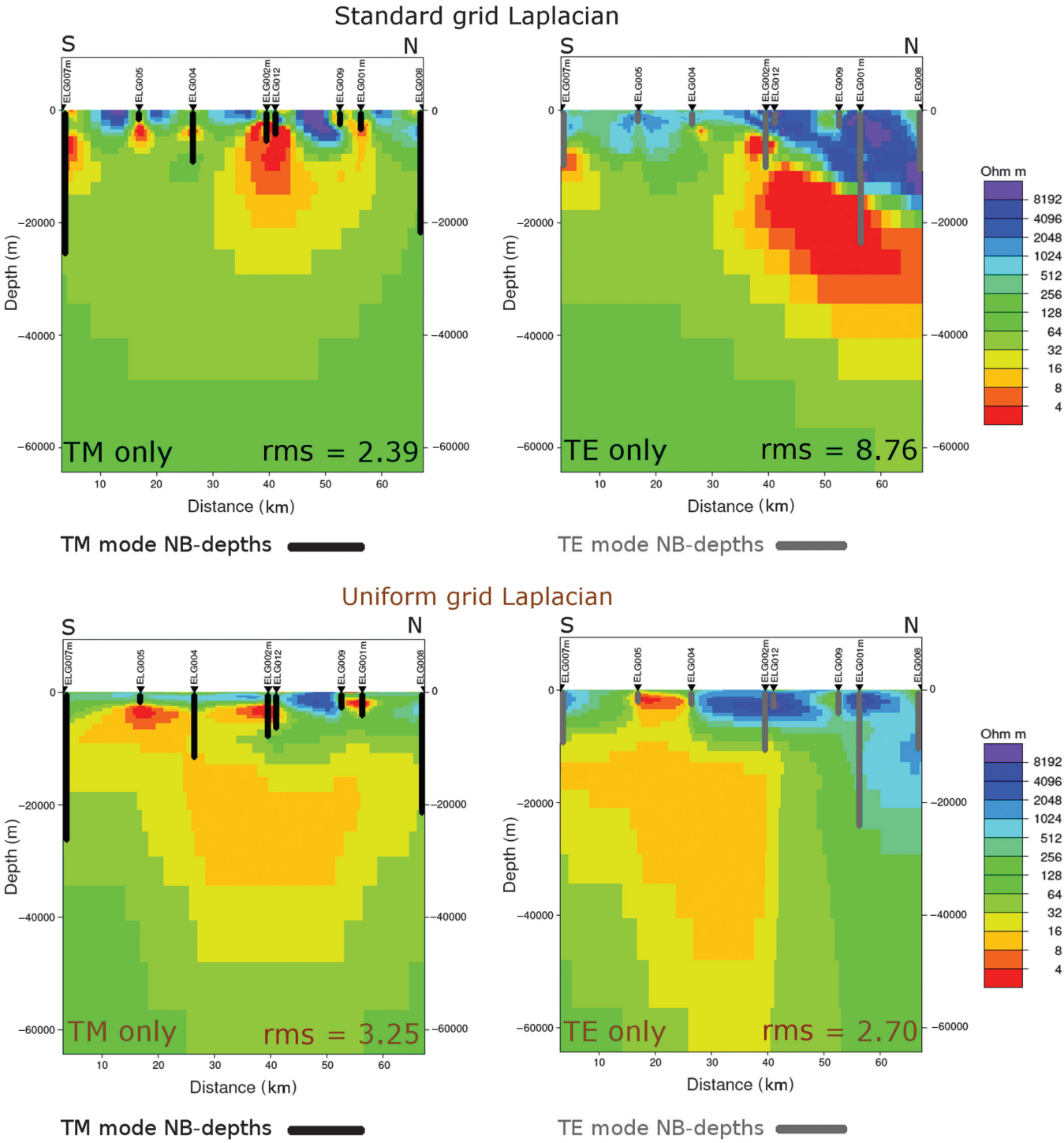

Figure 13. Standard grid (top) and uniform grid (bottom) Laplacian inversions for the individual TM (left) and TE (right) modes of the Otjiwarongo data. The standard grid Laplacian weighting factors were $\alpha = 1$, $\beta = 3$, $H = 500$ m, and $V = 500$ m and the uniform grid Laplacian weighting factors were; $\alpha = 1$, $\beta = 1$, $H = 0$ m, and $V = 0$ m. Also shown are the NB-depth estimates for the TE and TM modes.

Figure 15a and 15c shows that sites ELG012, ELG009, and ELG001m have large misfits, where large in this instance is defined as a misfit that is greater than the average rms error of the entire model, for the standard grid and uniform grid Laplacian inversions. Site ELG009 contains poor data estimates at several frequencies, explaining why it has the largest misfit, whereas the data from sites ELG001m and ELG012 probably still suffer from the effects of surficial conductive 3D structures. Interestingly, in terms of

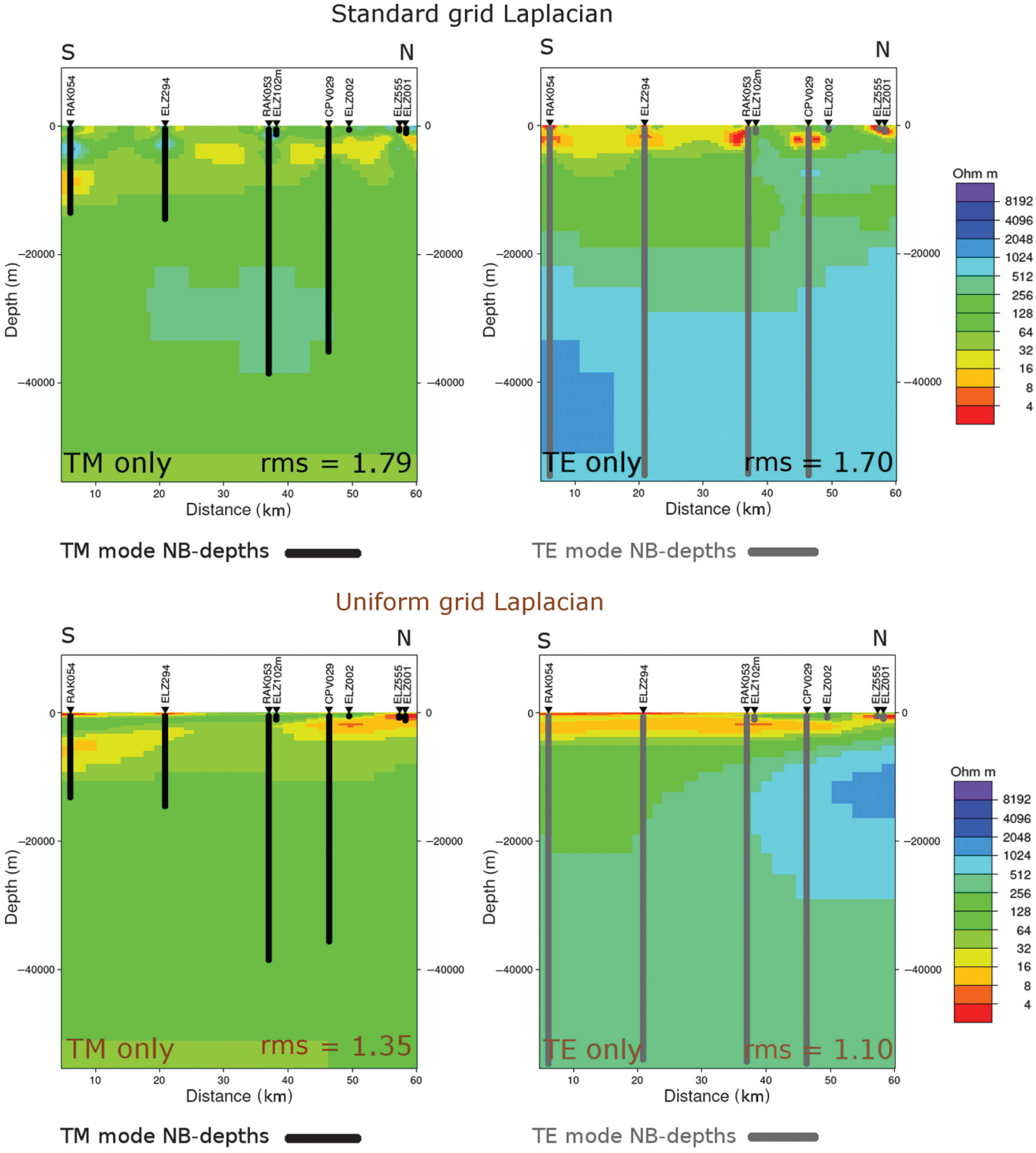

Figure 14. Standard grid (top) and uniform grid (bottom) Laplacian inversions for the individual TM (left) and TE (right) modes of the Katima Mulilo data. The standard grid Laplacian weighting factors were; $\alpha = 1$, $\beta = 3$, $H = 500$ m, and $V = 500$ m and the uniform grid Laplacian weighting factors were; $\alpha = 1$, $\beta = 1$, $H = 0$ m, and $V = 0$ m. Also shown are the NB-depth estimates for the TE and TM modes.

conductivity structure, the two models differ the most around sites ELG004 and ELG002m, which correlates well with site ELG004 having a large rms error in Figure 15a and a small error in Figure 15c, whereas the opposite applies for site ELG002m. The model differences, and subsequent differences in rms misfit, owe their origin to the standard grid and uniform grid Laplacian operators attempting to fit data that are biased by random noise (ELG002A and ELG004B had no remote sites and were locally processed) differently. This fact is also clear in the large discrepancy between the inverted static shift factors of, for example, site ELG004 (standard grid TM-SS = 8.39 and TE-SS = 2.41 versus uniform grid TM-SS = 3.41 and TE-SS = 1.08, Figure 15). Due to it being smoother (minimizing the risk of over interpreting a model) and fitting the data better (rms of 2.19 compared with 2.49), the uniform grid Laplacian inversion model with $\tau = 7$ was selected for further analysis instead of the standard grid Laplacian inversion model.

The chosen Otjiwarongo model has several interesting features, but there are two prominent ones to highlight. The first is a highly resistive upper crustal structure reaching a maximum depth of approximately 8 km between sites ELG012 and ELG009 that is interrupted by more conductive material beneath sites ELG005 and ELG004 (Figure 15). The second is a highly conductive midcrustal conductor that appears to be connected with the conductive material interrupting the shallow-resistive layer (Figure 15).

The robustness of the midcrustal conductor was tested first by replacing all resistivities included in the conductive region with 100 Ωm, running the inversion again (with the same regularization settings), and noting whether the conductor reappeared. The conductor did reappear and was similar in location and appearance to the original one and the inversion produced the same rms error (Figure 17). Second, the robustness of the conductor was tested by replacing all resistivities included in the conductive region by 100 Ωm, locking the altered cells, running the inversion again and forcing other parts of the model to change to try to produce the same rms error. The resultant inversion showed that there were no changes that could be made to the variable parts of the model to produce the previous rms error of 2.19, and instead a larger rms error of 4.55 was obtained (Figure 17). As was intuitively expected, sites ELG005, ELG004, and ELG002m contributed most to the increased average misfit, where their rms errors increased to 6.65, 5.10, and 6.72, respectively, compared with the errors in Figure 15c. The same two robustness tests were applied on the shallow-resistive layer with similar results. When the resistor was removed, it reappeared unaltered after inversion (rms error of 2.24), and when it was removed and the altered cells locked, no major changes were observed after inversion for the rest of the model, while the rms error increased to 14.71 (misfit for all sites increased to larger than 10).

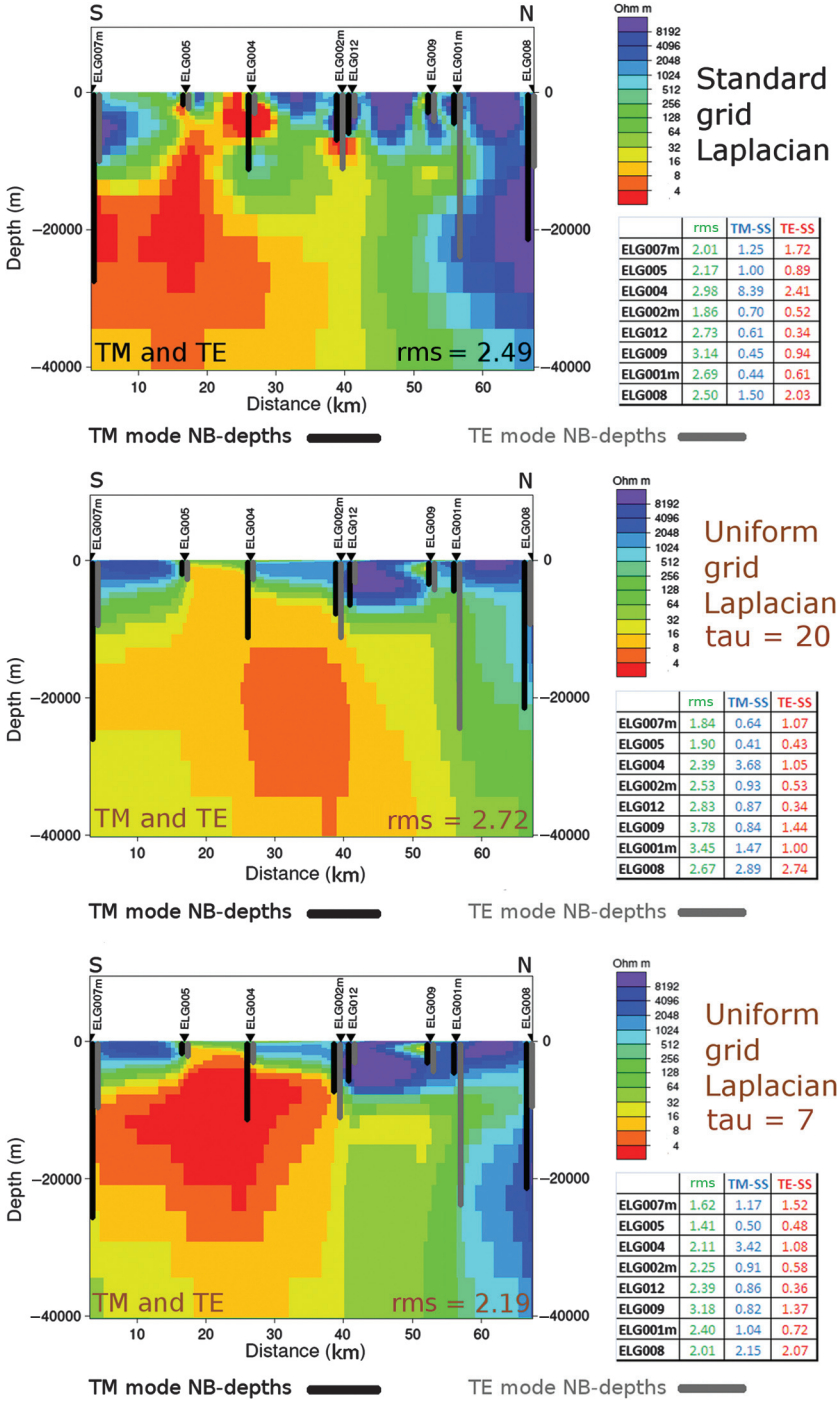

Figure 15. Standard grid (a) and uniform grid (b and c) Laplacian joint inversions of the TM and TE modes of the Otjiwarongo data. The standard grid Laplacian weighting factors were $\alpha = 1$, $\beta = 3$, $H = 500$ m, $V = 500$ m, and $\tau = 7$. The uniform grid Laplacian weighting factors were; $\alpha = 1$, $\beta = 1$, $H = 0$ m, $V = 0$ m, $\tau = 20$, and $\tau = 7$ for the middle and bottom results, respectively. Static shift inversion results for the TE (TE-SS) and TM (TM-SS) modes and individual rms errors for each of the eight sites are shown. Also shown are the NB-depth estimates for the TE and TM modes.

NB-depth estimates for the Otjiwarongo sites (Figure 15c) showed that deep structure has been added by regularization that is not required by the data. To emphasize the role of regularization, most of the midcrustal conductor was removed and still, after forward modeling, the rms error of the altered model remained 2.19 (Figure 18, left). In view of the fact that with MT the base of a conductor is not well resolved, and because of regularization, an attempt was made to reduce the effects of regularization by locking parts of the conductor that the data are sensitive to, and running the inversion again (Figure 18). The resultant inversion model (Figure 18, right) required less structure to be added to the conductor and its base is shallower than in the original model (Figure 15), and subsequently it was used in further analysis.

The uniform grid Laplacian inversion of the Katima Mulilo data is smoother and has a smaller rms error than the standard grid Laplacian inversion (Figure 16), and was, therefore, selected for further analysis. The most prominent feature in the chosen model is a shallow-conductive layer that is detected by all sites and reaches a maximum depth of approximately 6 km (Figure 16). The robustness of the shallow-conductive layer was tested, in a similar manner to the Otjiwarongo conductor, by first replacing all resistivities in the shallow subsurface with 100 Ωm, running the inversion again (with the same regularization settings) and seeing if the conductive layer reappeared. The conductive layer did reappear and was identical to the original and the rms error remained the same (Figure 19). Second, the shallow subsurface was given a value of 100 Ωm, the altered cells were locked, and the inversion was restarted. The second test result shows that although subtle changes were made to the rest of the model, the original rms error of 1.08 could not be achieved, and instead, the rms error increased to 15.03 (Figure 19). All sites contributed to the increased average misfit, with site ELZ102m (rms = 8.30) being the only site with an increased error less than 10.

The NB-depths of the TE and TM modes of the Katima Mulilo data (Figure 16) indicate that there is much greater depth sensitivity when compared with the Otjiwarongo data (Figure 15). However, because the spacing between some sites is large compared with the depth of the conductive layer, parts of the layer can still be removed keeping the rms error the same (Figure 20, left). To quantify the effects of regularization on the thickness and depth of the layer, only the parts of the model that the data are sensitive to were locked, similar to the Otjiwarongo conductor, and the inversion was run again (Figure 20). Unlike the Otjiwarongo inversion, the inversion result after locking the appropriate parts of the Katima Mulilo conductive layer was not different from the original inversion (compare Figures 16 and 20, right).

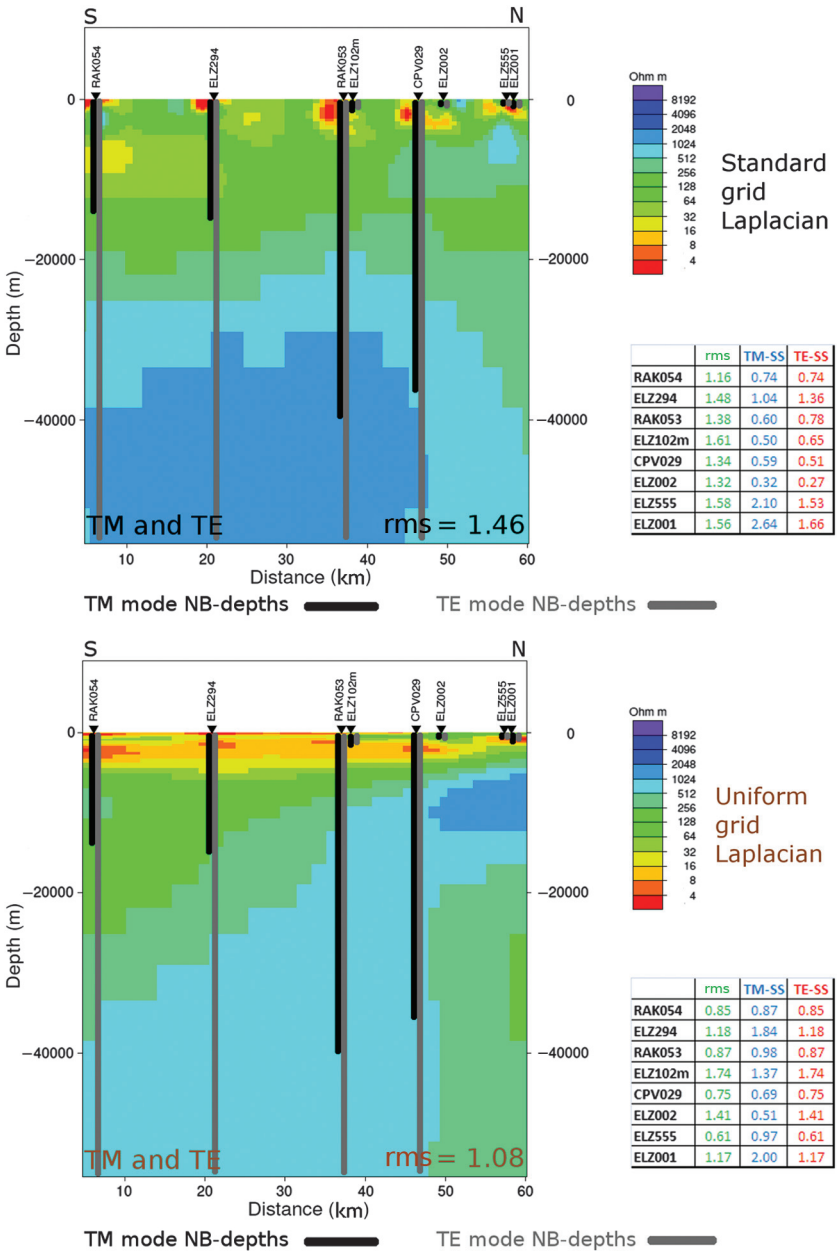

	rms	TM-SS	TE-SS
RAK054	1.16	0.74	0.74
ELZ294	1.48	1.04	1.36
RAK053	1.38	0.60	0.78
ELZ102m	1.61	0.50	0.65
CPV029	1.34	0.59	0.51
ELZ002	1.32	0.32	0.27
ELZ555	1.58	2.10	1.53
ELZ001	1.56	2.64	1.66

	rms	TM-SS	TE-SS
RAK054	0.85	0.87	0.85
ELZ294	1.18	1.84	1.18
RAK053	0.87	0.98	0.87
ELZ102m	1.74	1.37	1.74
CPV029	0.75	0.69	0.75
ELZ002	1.41	0.51	1.41
ELZ555	0.61	0.97	0.61
ELZ001	1.17	2.00	1.17

Figure 16. Standard grid (a) and uniform grid (b) Laplacian joint inversions of the TM and TE modes of the Katima Mulilo data. The standard grid Laplacian weighting factors were $\alpha = 1$, $\beta = 3$, $H = 500$ m, $V = 500$ m, and $\tau = 10$. The uniform grid Laplacian weighting factors were $\alpha = 1$, $\beta = 1$, $H = 0$ m, $V = 0$ m, and $\tau = 10$. Static shift inversion results for the TE (TE-SS) and TM (TM-SS) modes and individual rms errors for each of the eight sites are shown. Also shown are the NB-depth estimates for the TE and TM modes.

DISCUSSION

Placement of earth electrodes

The successful placement of an HVDC earth electrode depends on the conductivity of rock volumes near the surface and in close proximity to the electrode (Thunehed et al., 2007; J. H. de Beer, personal communication, 2009). Therefore, thorough evaluations of conductivity variations in the shallow subsurface associated with the Otjiwarongo and Katima Mulilo regions,

especially where AMT data are available, need to be completed before a decision on electrode placement is made.

It is clear from the two Otjiwarongo inversions (Figure 15), which are in agreement, that of all sites included in the inversions, the shallow subsurface is most conductive below sites ELG005 and ELG004. Despite similar structures surrounding sites ELG005 and ELG004 in the two models, the uniform grid Laplacian inversion is used for further testing because although in the standard grid

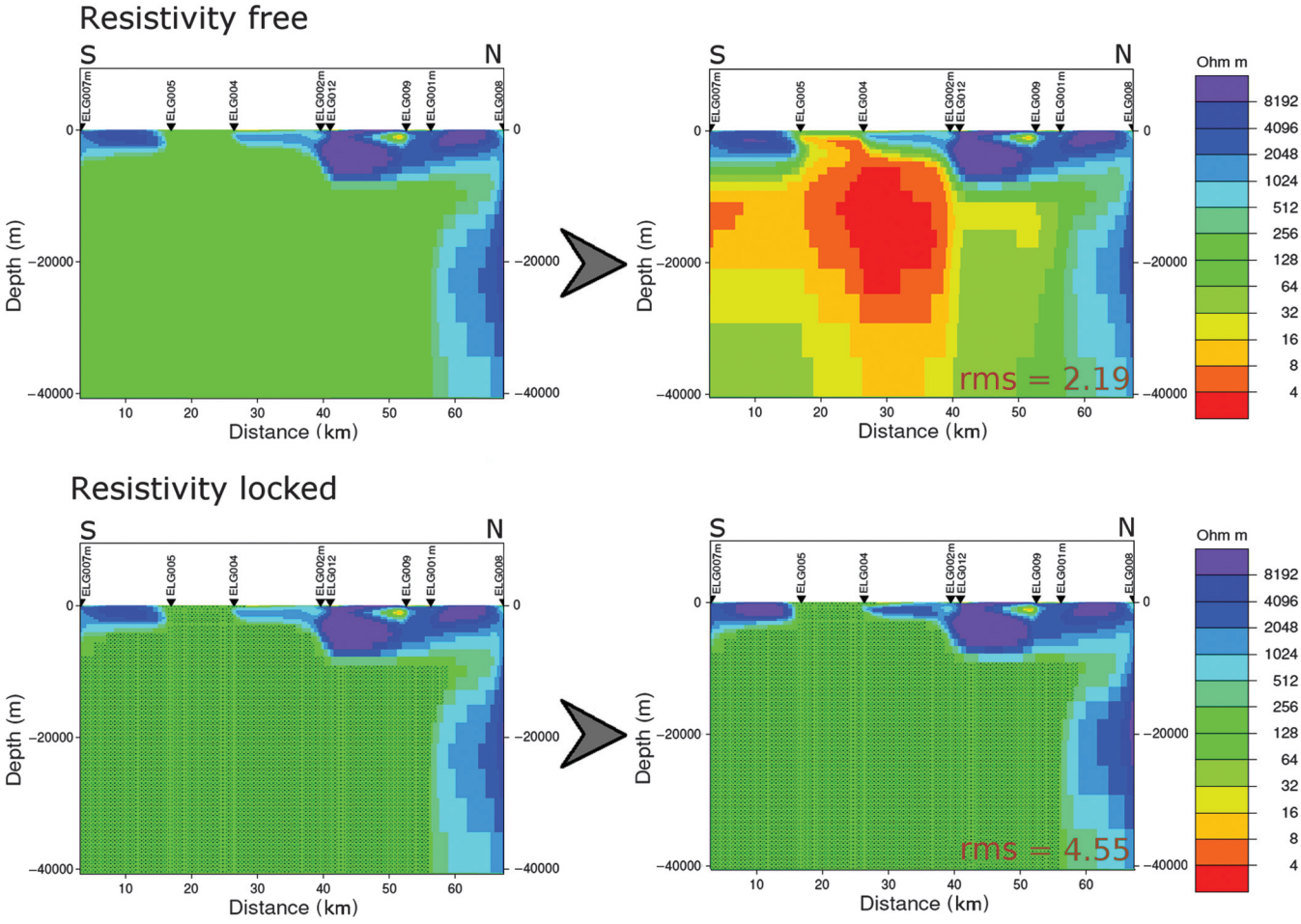

Figure 17. Sensitivity tests done on the Otjiwarongo inversion by first removing the midcrustal conductor, leaving all cells free to vary, and inverting again (top); and second, removing the conductor, leaving only cells outside the conductive region free, and inverting again (bottom).

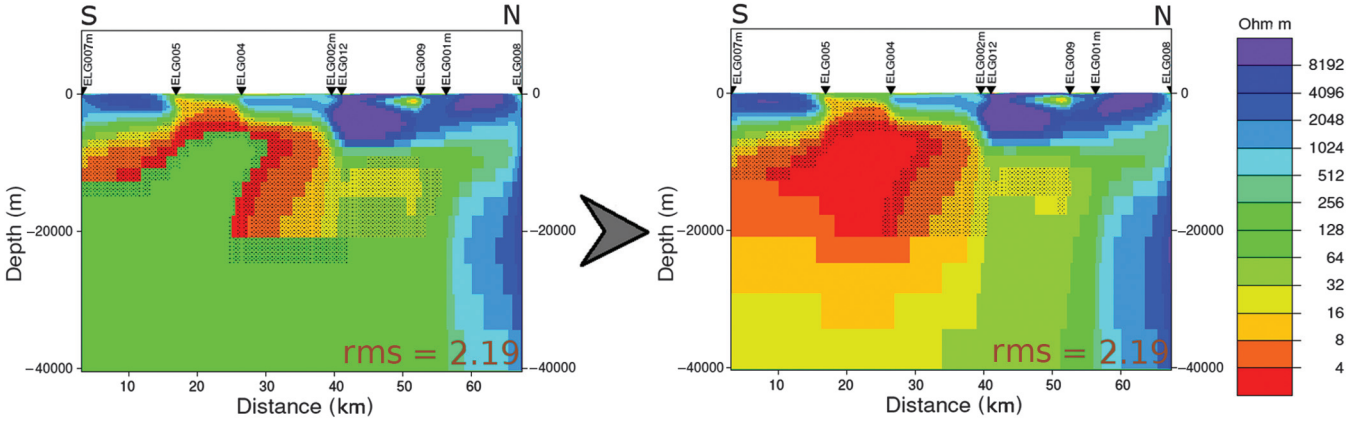

Figure 18. Locking only the parts of the midcrustal conductor that the Otjiwarongo data are sensitive to, and the inversion result with the appropriate cells locked (right).

Laplacian model greater emphasis is placed on resolving shallow structures, and the TM mode responses (providing information about conductivity boundaries) are not weighted down during inversion, sites ELG005 and ELG004 also have higher misfits (compared with neighboring sites) in the latter model. The robustness of the high conductivity beneath sites ELG005 and ELG004 in Figure 15c was tested by assigning 5000 Ωm resistivities to all cells greater than 5 km depth and running the inversion again (using the same inversion settings) (Figure 21a). The resulting model shows that across the profile the conductivity remains the highest beneath sites ELG005 and ELG004 (Figure 21a).

According to the currently available geologic information in the Otjiwarongo region, site ELG004 is situated on an undifferentiated Damara sequence (NDA in Figure 4), whereas site ELG005 is located on Nosib group rocks, consisting of quartzite, arkose with conglomerate, and ironstone (NNS in Figure 4). It is unclear what the cause of the high conductivity beneath site ELG004 is, whereas prior studies have determined that the several dome structures

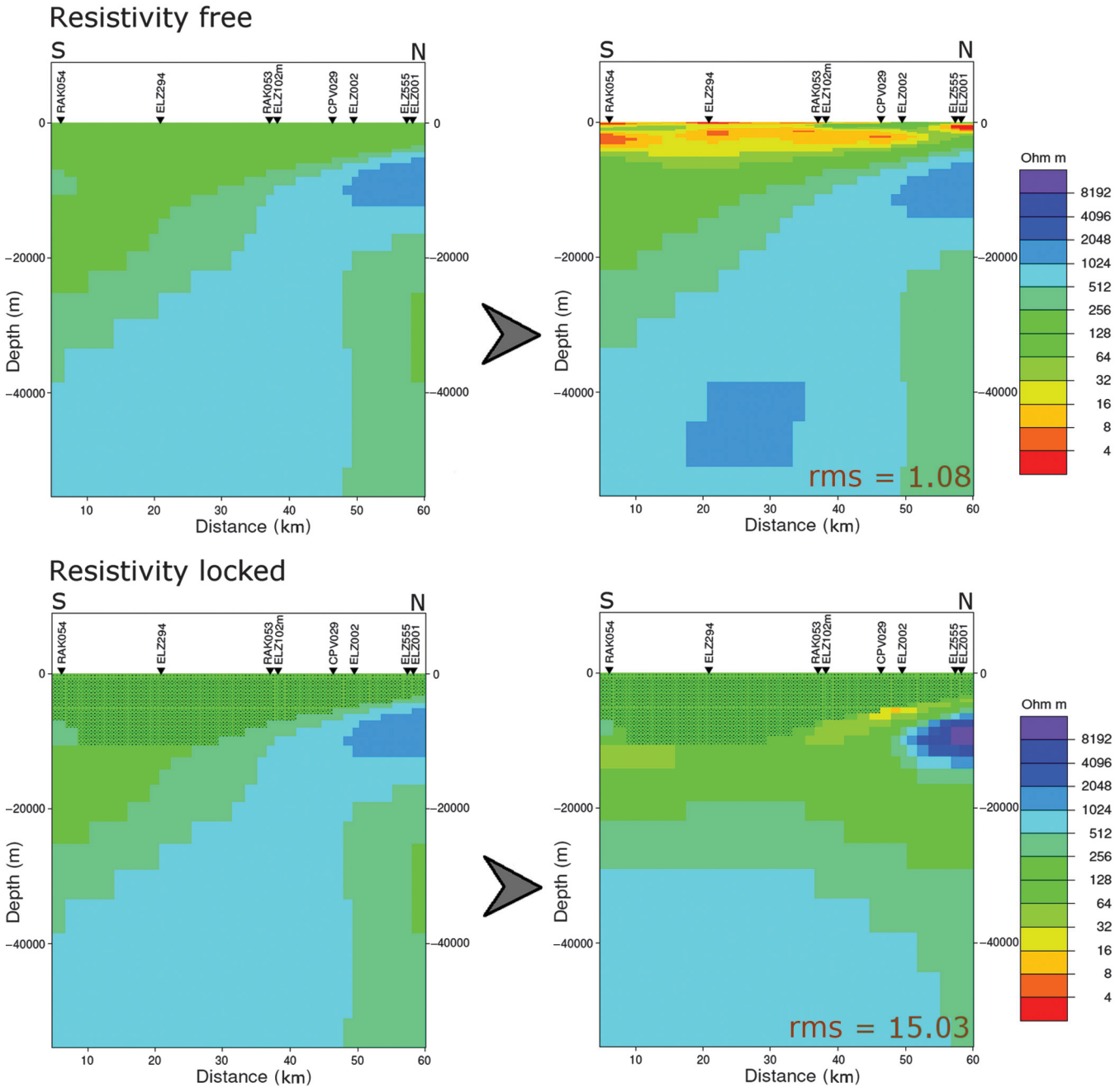

Figure 19. Sensitivity tests done on the Katima Mulilo inversion by first removing the shallow-conductive layer, leaving all cells free to vary, and inverting again (top); and second, removing the conductive layer, leaving only cells below the layer free to vary, and inverting again (bottom).

located southwest of Otjiwarongo, and underlying site ELG005, carry in excess of 4% graphite (Miller, 2008, p. 13–31). Therefore, site ELG005, rather than site ELG004, is proposed as an optimal location to place the HVDC earth electrode in the Otjiwarongo region.

Similar to the Otjiwarongo region, the robustness of all conductive structures present in the Katima Mulilo uniform grid inversion model was tested by substituting all resistivities in the shallow subsurface (up to 1 km) with a thin 5000-Ωm layer and inverting again (using the same inversion settings) (Figure 21b). The resulting inversion model is similar to the original and both show that beneath sites RAK054, ELZ294, RAK053, ELZ102m, and CPV029 the conductivity is highest (Figure 21b).

Owing to the lack of detailed geologic information in the Katima Mulilo region, attributed to the vast Kalahari sediment cover (Moore and Larkin, 2001; Singletary et al., 2003), geology cannot be used to facilitate the choice of an appropriate electrode location. A choice based solely on the conductivity information gathered from the MT data must be made. Due to the approximate 1D behavior of data in the AMT frequency range (Figure 8b), 1D inversion tools can be used to observe conductivity variations with depth below each site. The 1D behavior is especially prevalent in the uppermost subsurfaces (only low frequencies in Table 1 show higher dimensional characteristics), which correlates well with the expected layered sedimentary environment (Kalahari sediments and Karoo sediments and basalts). Subsequently, NB resistivities (Niblett and Sayn-Wittgenstein, 1960; Bostick, 1977) were computed for the AMT sites at depths of 100, 200, 500, 900, and 1000 m (Figure 22). The 1D inversion results show that the conductivities of regions including sites ELZ102m and ELZ103 are consistently high at all depths calculated (Figure 22). Other sites also have highly conductive subsurfaces (as expected), but the conductivities are not consistently high at all depths. In addition, at the shallowest modeled depth (i.e., 100 m), the conductivity beneath site ELZ103 is highest.

The shallow subsurface beneath ELZ102m was also indicated as highly conductive in the 2D inversion model. Its neighboring site in the model RAK053, which had a similar high conductivity subsurface, is situated, in plan view (Figure 11b), between it and site ELZ103. In light of the similarities between 1D and 2D inversions of the Katima Mulilo data, regarding the high conductivity shallow subsurfaces beneath sites ELZ102m, RAK053, and ELZ103, the region enclosing the three sites is deemed most appropriate for earth electrode placement.

Interpretation of 2D inversion results

The Otjiwarongo area is characterized by large volumes of metamorphic rocks and sparse intrusive igneous complexes (Figure 4). By combining knowledge of geology and the factors controlling conductivity, it can be concluded that resistive shallow rocks, as measured, are unfractured (not fluid-filled, van Zijl and de Beer, 1983), and do not contain interconnected highly conductive materials. The same metamorphic rocks exposed at the surface continue to midcrustal depths (Gray et al., 2006), but, in contrast, the conductivity, along most of the 2D profile (Figure 15), increases significantly. The temperature at midcrustal depths is too low for the conductivity to be increased by semiconduction, and the presence of large quantities of fluid can be ruled out due to high pressures. Although there has been volcanic activity in the past (attested by the presence of igneous intrusions, Figure 7a) there is none at present. Thus, the presence of partial melt can also be ruled out as a possible cause of the high conductivity.

A comparison of localities of the Otjiwarongo array and the conductive belt in northern Namibia and Botswana indicates that most of the array overlies the belt (Figure 6b). The Otjiwarongo conductor is also situated at the same midcrustal depth range characteristic of the conductive belt. Therefore, it can be confidently concluded that the conductive belt exists below the Otjiwarongo area and the MT data have substantiated its existence. The materials suggested to

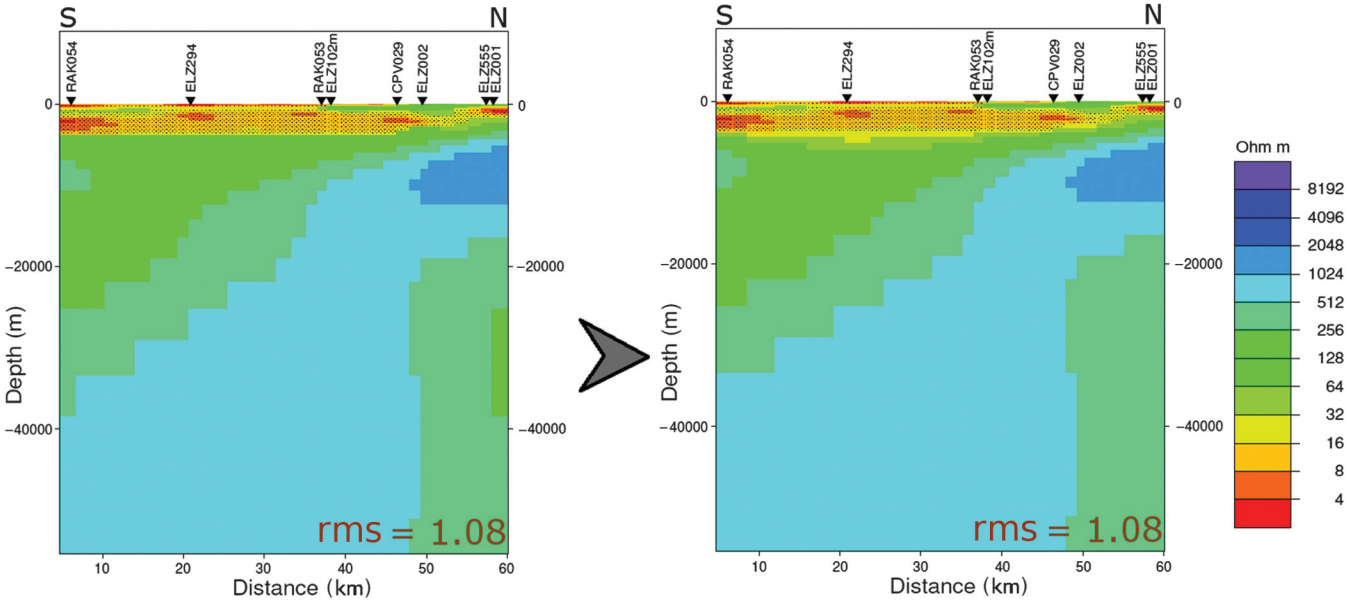

Figure 20. Locking only the parts of the conductive layer that the Katima Mulilo data are sensitive to, and the inversion result with the appropriate cells locked (right).

be the cause of high conductivities observed in the belt, were magnetite (produced by serpentinization of the DMB rocks, van Zijl and de Beer, 1983) and graphite, correlated with marble units present in shear zones (Ritter et al., 2003). In the Otjiwarongo region, marble units (NSWm in Figure 4) are also present, and are contained in undifferentiated Swakop group rocks associated with the regional shear zone traversing the study area. The shear zone manifests itself, on the surface, as the Othohorongo thrust, which is the southwest extension of the same shear zone, which intersected the MT profile of Ritter et al. (2003), namely the Autseib Fault (Figure 7a). Hence, it is concluded that interconnected graphite is also associated with marble units in the Otjiwarongo region, and it is the cause of the high conductivity of the midcrustal conductor.

High conductivities at the uppermost subsurface of the Katima Mulilo area (Figure 16) are attributed to porous sediments of the Kalahari group. However, Kalahari sediments in the area have a maximum thickness of 100–200 m (Thomas and Shaw, 1990), and therefore, there exists an alternate reason for the high conductivities observed deeper down. A cause similar to the one responsible for the DMB conductive belt appears unlikely because the Katima Mulilo area does not coincide with any region covered by the conductive belt (Figure 6b), and the Katima Mulilo conductive layer is confined to the upper crust, whereas the belt is a midcrustal phenomenon. Near horizontal shear zones could be present, and the materials found within the shear zones could be causing the anomaly. Due to the high grades of metamorphism present in the DMB (which also increases to the northwest; Singletary et al., 2003), it can be deduced that horizontal shear zones are implausible and near vertical ones more realistic.

Clastic and carbonate rocks of the Ghanzi group, existing within the Northwest Botswana rift, directly underlie the Kalahari sediments (Figure 5). It is possible that the clastic and carbonate rocks are fractured and fluid-filled at upper crustal depths, but in Namibia the shallow DMB rocks have been found to be unfractured (van Zijl and de Beer, 1983; Ritter et al., 2003), and the depositional and deformational histories of DMB rocks in Namibia and Botswana are alike. The Ghanzi group is, in part, an extension of the Nosib group, which contains localized ironstone (Tankard et al., 1982,

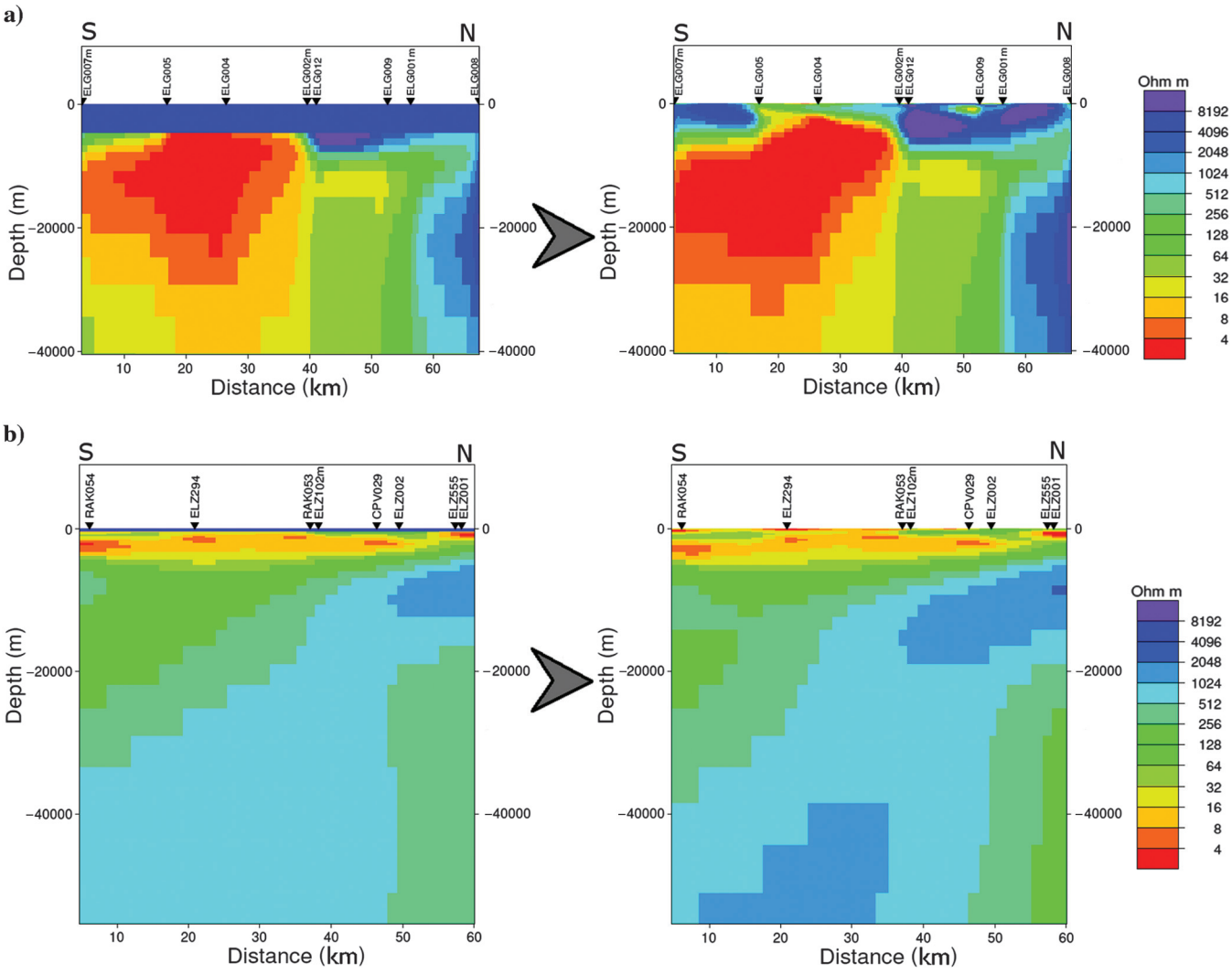

Figure 21. (a) Uniform grid Laplacian inversion result (right) after placing a 5-km-thick resistive layer at the top of the original Otjiwarongo inversion model (left) and (b) uniform grid Laplacian inversion result (right) after placing a thin 1-km resistive layer at the top of the original Katima Mulilo inversion model (left).

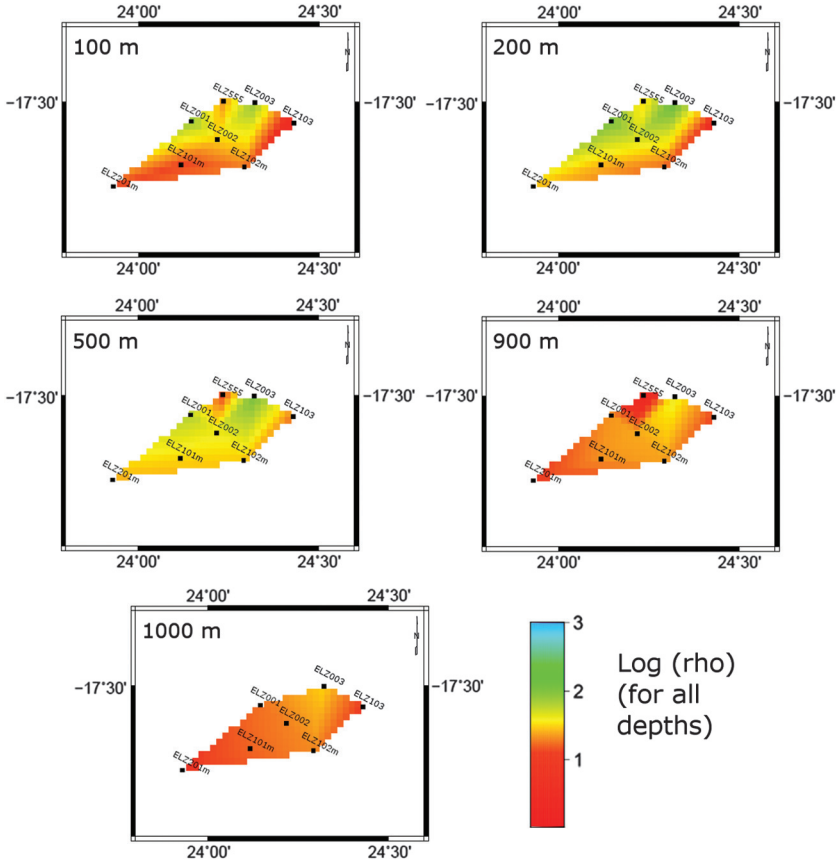

Figure 22. NB-resistivities calculated for the Katima Mulilo AMT sites at depths of 100, 200, 500, 900, and 1000 m.

p. 317) and in some instances large amounts of graphite (southwest of Otjiwarongo, Miller, 2008, pp. 13–31). Ironstone has also been discovered in the mobile belts in Botswana (Hutchins and Reeves, 1980; Kampunzu et al., 2000). The hypothesis is, therefore, formulated that ironstone and/or graphite is present in the Ghanzi group rocks forming the basement beneath the Katima Mulilo area, and it is the cause of the observed high conductivity at upper crustal depths (not including the shallowest depths). The conductive layer can, in part, also be due to conductive materials located within the Karoo basin sediments. This could explain the 1D layered nature of the conductive feature in the Katima Mulilo region. To determine which possibility is more plausible, drilling will be needed in the area.

CONCLUSION

Inversions models have been derived from MT data of the Otjiwarongo and Katima Mulilo regions, Namibia. Analyses of the surficial conductivities of the Otjiwarongo and Katima Mulilo areas show that areas around site ELG005, close to Otjiwarongo, and sites ELZ102m, RAK053, and ELZ103, close to Katima Mulilo, are optimal locations for HVDC earth electrode placement. At greater crustal depth, the most prominent feature of the Otjiwarongo 2D models, a midcrustal conductor, was deduced to be caused by graphite associated with marble units in a local shear zone. The Katima Mulilo 2D inversion detected an upper crustal high-conductivity layer. The uppermost 200 m of the layer, and its related high conductivity, is attributed to the thick sedimentary Kalahari cover in the area (porous and fluid-filled), whereas the cause of the conductivity deeper down (to a depth of 6–7 km) remains enigmatic. It is possible that ironstone or graphite present in the basement rocks could be the cause, due to the discovery of such elements in similar rock types in other parts of the DMB. However, such a hypothesis needs to be tested, preferably by drilling.

ACKNOWLEDGMENTS

The first author's research was sponsored by Council for Scientific and Industrial Research, South Africa. We would like to acknowledge the entire SAMTEX team for their hard work and assistance throughout the entire length of the project. Also, the authors would like to express their gratitude to H. Thunehed and J. de Beer for informative discussions on the content of the paper. Last, the authors acknowledge and thank three anonymous reviewers of the paper and the associate editor for very insightful comments and suggestions.

REFERENCES

Begg, G. C., W. L. Griffin, L. M. Natapov, S. Y. O'Reilly, S. P. Grand, C. J. O'Neill, J. M. A. Hronsky, Y. Poudjom Djomani, C. J. Swain, T. Deen, and P. Bowden, 2009, The lithospheric architecture of Africa: Seismic tomography, mantle petrology, and tectonic evolution: Geosphere, **5**, 23–50, doi: 10.1130/GES00179.1.

Berdichevsky, M. N., 1999, Marginal notes on magnetotellurics: Surveys in Geophysics, **20**, 341–375, doi: 10.1023/A:1006645715819.

Boschi, L., T. W. Becker, G. Soldati, and A. M. Dziewonski, 2006, On the relevance of Born theory in global seismic tomography: Geophysical Research Letters, **33**, 1–4, doi: 10.1029/2005GL025063.

Bostick, F. X., 1977, A simple almost exact method of MT analysis: Workshop on Electrical Methods in Geothermal Exploration, U.S. Geological Survey Contract Number 14080001-8-359.

Cagniard, L., 1953, Basic theory of the magneto-telluric method of geophysical prospecting: Geophysics, **18**, 605–635, doi: 10.1190/1.1437915.

Catuneanu, O., H. Wopfner, P. G. Eriksson, B. Cairncross, B. S. Rubidge, R. M. H. Smith, and P. J. Hancox, 2005, The Karoo basins of south-central Africa: Journal of African Earth Sciences, **43**, 211–253, doi: 10.1016/j.jafrearsci.2005.07.007.

Chave, A. D., and A. G. Jones, 1997, Electric and magnetic field galvanic distortion decomposition of BC87 data: Journal of Geomagnetism and Geoelectricity, **49**, 767–789, doi: 10.5636/jgg.49.767.

Chave, A. D., and A. G. Jones, 2012, The magnetotelluric method — Theory and practice: Cambridge University Press.

Coward, M. P., and M. C. Daly, 1984, Crustal lineaments and shear zones in Africa: Their relationship to plate movements: Precambrian Research, **24**, 27–45, doi: 10.1016/0301-9268(84)90068-8.

Daly, M. C., 1986, Crustal shear zones and thrust belts: Their geometry and continuity in Central Africa: Philosophical Transactions of the Royal Society of London, **317**, 111–128, doi: 10.1098/rsta.1986.0028.

de Beer, J. H., R. M. J. Huyssen, S. J. Joubert, and J. S. V. van Zijl, 1982, Magnetometer array studies and deep Schlumberger soundings in the Damara orogenic belt, south west Africa: Geophysical Journal of the Royal Astronomical Society, **70**, 11–29, doi: 10.1111/j.1365-246X.1982.tb06388.x.

de Beer, J. H., J. S. V. van Zijl, R. M. J. Huyssen, P. L. V. Hugo, S. J. Joubert, and R. Meyer, 1976, A magnetometer array study in south-west Africa, Botswana and Rhodesia: Geophysical Journal of the Royal Astronomical Society, **45**, 1–17, doi: 10.1111/j.1365-246X.1976.tb00310.x.

de Groot-Hedlin, C., 1991, Removal of static shift in two dimensions by regularized inversion: Geophysics, **56**, 2102–2106, doi: 10.1190/1.1443022.

Evans, R. L., A. G. Jones, X. Garcia, M. R. Muller, M. P. Hamilton, S. Evans, C. J. S. Fourie, J. Spratt, S. J. Webb, H. Jelsma, and D. Hutchins, 2011, The electrical lithosphere beneath the Kaapvaal Craton, Southern Africa: Journal of Geophysical Research, **116**, B04105, doi: 10.1029/2010JB007883.

Fullea, J., M. R. Muller, and A. G. Jones, 2011, Electrical conductivity of continental lithospheric mantle from integrated geophysical and petrological modeling: Application to the Kaapvaal Craton and Rehoboth Terrane, southern Africa: Journal of Geophysical Research, **116**, B10202, doi: 10.1029/2011JB008544.

Gamble, T. D., W. M. Goubau, and J. Clarke, 1979, Magnetotellurics with a remote magnetic reference: Geophysics, **44**, 53–68, doi: 10.1190/1.1440923.

Garcia, X., and A. G. Jones, 2002, Atmospheric sources for audiomagnetotelluric (AMT) sounding: Geophysics, **67**, 448–458, doi: 10.1190/1.1468604.

Gray, D. R., D. A. Foster, B. C. Goscombec, W. Passchier, and R. A. J. Trouwe, 2006, 40Ar/39Ar thermochronology of the Pan-African Damara Orogen, Namibia, with implications for tectonothermal and geodynamic evolution: Precambrian Research, **150**, 49–72, doi: 10.1016/j.precamres.2006.07.003.

Groom, R. W., and K. Bahr, 1992, Corrections for near surface effects: Decomposition of the magnetotelluric impedance tensor and scaling corrections for regional resistivities: A tutorial: Surveys in Geophysics, **13**, 341–379, doi: 10.1007/BF01903483.

Groom, R. W., and R. C. Bailey, 1989, Decomposition of magnetotelluric impedance tensors in the presence of local three-dimensional galvanic distortion: Journal of Geophysical Research, **94**, 1913–1925, doi: 10.1029/JB094iB02p01913.

Hamilton, M. P., A. G. Jones, R. L. Evans, S. Evans, C. J. S. Fourie, X. Garcia, A. Mountford, and J. E. Spratt, and the SAMTEX Team, 2006, Electrical anisotropy of South African lithosphere compared with seismic anisotropy from shear-wave splitting analyses: Physics of the Earth and Planetary Interiors, **158**, 226–239, doi: 10.1016/j.pepi.2006.03.027.

Hansen, P. C., 1992, Analysis of discrete ill-posed problems by means of the L-curve: SIAM Review, **34**, 561–580, doi: 10.1137/1034115.

Hutchins, D. G., and C. V. Reeves, 1980, Regional geophysical exploration of the Kalahari in Botswana: Tectonophysics, **69**, 201–220, doi: 10.1016/0040-1951(80)90211-5.

Jacobs, J., S. Pisarevsky, R. J. Thomas, and T. Becker, 2008, The Kalahari craton during the assembly and dispersal of Rodinia: Precambrian Research, **160**, 142–158, doi: 10.1016/j.precamres.2007.04.022.

Jones, A. G., 1983a, On the equivalence of the Niblett and Bostick transformations in the magnetotelluric method: Journal of Geophysics, **53**, 72–73.

Jones, A. G., 1983b, The problem of "current channelling": A critical review: Geophysical Surveys (now Surveys in Geophysics), **6**, 79–122, doi: 10.1007/BF01453996.

Jones, A. G., 1999, Imaging the continental upper mantle using electromagnetic methods: Lithos, **48**, 57–80, doi: 10.1016/S0024-4937(99)00022-5.

Jones, A. G., A. D. Chave, G. Egbert, D. Auld, and K. Bahr, 1989, A comparison of techniques for magnetotelluric response function estimation: Journal of Geophysical Research, **94**, 14201–14213, doi: 10.1029/JB094iB10p14201.

Jones, A. G., R. L. Evans, and D. W. Eaton, 2009a, Velocity-conductivity relationships for mantle mineral assemblages in Archean cratonic lithosphere based on a review of laboratory data and Hashin-Shtrikman extremal bounds: Lithos, **109**, 131–143, doi: 10.1016/j.lithos.2008.10.014.

Jones, A. G., R. L. Evans, M. R. Muller, M. P. Hamilton, M. P. Miensopust, X. Garcia, P. Cole, T. Ngwisanyi, D. Hutchins, C. J. S. Fourie, H. Jelsma, T. Aravanis, W. Pettit, S. J. Webb, and J. Wasborg, the SAMTEX Team, 2009b, Area selection for diamonds using magnetotellurics: Examples from southern Africa: Lithos, **112S**, 83–92, doi: 10.1016/j.lithos.2009.06.011.

Jones, A. G., S. Fishwick, R. L. Evans, M. R. Muller, and J. Fullea, 2013, Velocity-conductivity relations for cratonic lithosphere and their application: Example of Southern Africa: Geochemistry, Geophysics, Geosystems, **14**, 806–827, doi: 10.1002/ggge.20075.

Jones, A. G., J. Fullea, R. L. Evans, and M. R. Muller, 2012, Water in cratonic lithosphere: Calibrating laboratory-determined models of electrical conductivity of mantle minerals using geophysical and petrological observations: Geochemistry, Geophysics, Geosystems, **13**, Q06010, doi: 10.1029/2012GC004055.

Kampunzu, A. B., R. A. Armstrong, M. P. Modisi, and R. B. M. Mapeo, 2000, Ion microprobe U-Pb ages on detrital zircon grains from the Ghanzi Group: Implications for the identification of a Kibaran-age crust in northwest Botswana: Journal of African Earth Sciences, **30**, 579–587, doi: 10.1016/S0899-5362(00)00040-3.

Key, R. M., and C. C. Rundle, 1981, The regional significance of new isotopic ages from Precambrian windows through the "Kalahari Beds" in northwestern Botswana: Transactions of the Geological Society of South Africa, **84**, 51–66.

Khoza, D., A. G. Jones, M. R. Muller, R. L. Evans, S. J. Webb, and M. Miensopust, the SAMTEX Team, 2013, Tectonic model of the Limpopo belt: Constraints from magnetotelluric data: Precambrian Research, **226**, 143–156, doi: 10.1016/j.precamres.2012.11.016.

Martin, H., and H. Porada, 1977, The intracratonic branch of the Damara Orogen in southwest Africa: I. Discussion of geodynamic models: Precambrian Research, **5**, 311–338, doi: 10.1016/0301-9268(77)90039-0.

McNeice, G. W., and A. G. Jones, 2001, Multisite, multifrequency tensor decomposition of magnetotelluric data: Geophysics, **66**, 158–173, doi: 10.1190/1.1444891.

Miensopust, M. P., A. G. Jones, M. R. Muller, X. Garcia, and R. L. Evans, 2011, Lithospheric structures and Precambrian terrane boundaries in northeastern Botswana revealed through magnetotelluric profiling as part of the Southern African Magnetotelluric Experiment: Journal of Geophysical Research, **116**, B02401, doi: 10.1029/2010JB007740.

Miller, R. M., 1983, The Pan-African Damara Orogen of Namibia: Special Publication of the Geological Society of South Africa, **11**, 431–515.

Miller, R. M., 2008, The geology of Namibia: Ministry of Mines and Energy: Geological survey of Namibia.

Modie, B. N., 2000, Geology and mineralisation in the Meso- to Neoproterozoic Ghanzi-Chobe belt of northwest Botswana: Journal of African Earth Sciences, **30**, 467–474, doi: 10.1016/S0899-5362(00)00032-4.

Moore, A. E., and P. A. Larkin, 2001, Drainage evolution in south-central Africa since the breakup of Gondwana: South African Journal of Geology, **104**, 47–68.

Muller, M. R., A. G. Jones, R. L. Evans, H. S. Grütter, C. Hatton, X. Garcia, M. P. Hamilton, M. P. Miensopust, P. Cole, T. D. Ngwisanyi, D. Hutchins, C. J. S. Fourie, H. A. Jelsma, S. F. Evans, T. Aravanis, W. Pettit, S. J. Webb, and J. Wasborg, and the SAMTEX Team, 2009, Lithospheric structure, evolution and diamond prospectivity of the Rehoboth Terrane and western Kaapvaal Craton, southern Africa: Constraints from broadband magnetotellurics: Lithos, **112S**, 93–105, doi: 10.1016/j.lithos.2009.06.023.

Nguuri, T. K., J. Gore, D. E. James, S. J. Webb, C. Wright, T. G. Zengeni, O. Gwavava, and J. A. Snoke, and the Kaapvaal Seismic Group, 2001, Crustal structure beneath southern Africa and its implications for the formation and evolution of the Kaapvaal and Zimbabwe cratons: Geophysical Research Letters, **28**, 2501–2504, doi: 10.1029/2000GL012587.

Niblett, E. R., and C. Sayn-Wittgenstein, 1960, Variation of electrical conductivity with depth by the magneto-telluric method: Geophysics, **25**, 998–1008, doi: 10.1190/1.1438799.

Nover, G., 2005, Electrical properties of crustal and mantle rocks — A review of laboratory measurements and their explanation: Surveys in Geophysics, **26**, 593–651, doi: 10.1007/s10712-005-1759-6.

Olhoeft, G. R., 1981, Electrical properties of granite with implications for the lower crust: Journal of Geophysical Research, **86**, 931–936, doi: 10.1029/JB086iB02p00931.

Pakhomenko, E. I., B. P. Belikov, and E. Dvorzhak, 1973, Influence of serpentinization upon the elastic and electrical properties of rocks: Izvestiya Earth Physics, **8**, 101–108.

Reynard, B., K. Mibe, and B. van de Moortele, 2011, Electrical conductivity of the serpentinised mantle and fluid flow in subduction zones: Earth and Planetary Science Letters, **307**, 387–394, doi: 10.1016/j.epsl.2011.05.013.

Ritter, O., V. Haak, V. Rath, E. Stein, and M. Stiller, 1999, Very high electrical conductivity beneath the Münchberg Gneiss area in southern Germany: Implications for horizontal transport along shear planes: Geophysical Journal International, **139**, 161–170, doi: 10.1046/j.1365-246X.1999.00937.x.

Ritter, O., U. Weckmann, T. Vietor, and V. Haak, 2003, A magnetotelluric study of the Damara Belt in Namibia 1. Regional scale conductivity anomalies: Physics of the Earth and Planetary Interiors, **138**, 71–90, doi: 10.1016/S0031-9201(03)00078-5.

Roberts, J. J., and J. A. Tyburczy, 1999, Partial-melt electrical conductivity: Influence of melt composition: Journal of Geophysical Research, **104**, 7055–7065, doi: 10.1029/1998JB900111.

Rodi, W., and R. L. Mackie, 2001, Nonlinear conjugate gradients algorithm for 2-D magnetotelluric inversion: Geophysics, **66**, 174–187, doi: 10.1190/1.1444893.

Schwalenberg, K., V. Rath, and V. Haak, 2002, Sensitivity studies applied to a two-dimensional resistivity model from the central Andes: Geophysical Journal International, **150**, 673–686, doi: 10.1046/j.1365-246X.2002.01734.x.

Shankland, T. J., 1975, Electrical conduction in rocks and minerals: Parameters for interpretation: Physics of the Earth and Planetary Interiors, **10**, 209–219, doi: 10.1016/0031-9201(75)90047-3.

Singletary, S. J., R. E. Hanson, M. W. Martin, J. L. Crowley, S. A. Bowring, R. M. Key, L. V. Ramokate, B. B. Direng, and M. A. Krol, 2003, Geochronology of basement rocks in the Kalahari Desert, Botswana, and implications for regional Proterozoic tectonics: Precambrian Research, **121**, 47–71, doi: 10.1016/S0301-9268(02)00201-2.

Stesky, R. M., and W. F. Brace, 1973, Electrical conductivity of serpentinized rocks to 6 kilobars: Journal of Geophysical Research, **78**, 7614–7621, doi: 10.1029/JB078i032p07614.

Tankard, A. J., D. K. Hobday, M. P. A. Jackson, D. R. Hunter, K. A. Eriksson, and W. E. L. Minter, 1982, Crustal evolution of Southern Africa: 3.8 billion years of earth history: Springer-Verlag.

Thomas, D. S. G., and P. A. Shaw, 1990, The deposition and development of the Kalahari Group sediments, Central Southern Africa: Journal of African Earth Sciences, **10**, 187–197, doi: 10.1016/0899-5362(90)90054-I.

Thunehed, H., U. Åström, and B. Westman, 2007, Geophysical and geological preinvestigations for HVDC-electrodes: Presented at IEEE Power Engineering Society Conference and Exposition, 384–386.

Utada, H., and H. Munekane, 2000, On galvanic distortion of regional three-dimensional magnetotelluric impedances: Geophysical Journal International, **140**, 385–398, doi: 10.1046/j.1365-246x.2000.00014.x.

van Zijl, J. S. V., and J. H. de Beer, 1983, Electrical conductivity of the Damara Orogen and its tectonic significance: Special Publication of the Geological Society of South Africa, **11**, 369–379.

Wannamaker, P. E., G. W. Hohmann, and S. H. Ward, 1984, Magnetotelluric responses of three-dimensional bodies in layered earths: Geophysics, **49**, 1517–1533, doi: 10.1190/1.1441777.

Weckmann, U., O. Ritter, and V. Haak, 2003, A magnetotelluric study of the Damara Belt in Namibia: 2. MT phases over 90° reveal the internal structure of the Waterberg Fault/Omaruru Lineament: Physics of the Earth and Planetary Interiors, **138**, 91–112, doi: 10.1016/S0031-9201(03)00079-7.